Nano Research

Open Access

Review Article

Modification strategies on nickel-based electrocatalysts for energy-efficient anodic reactions

Jingwen Yu, Yunliang Liu, Naiyun Liu ✉, Yaxi Li, Yuanyuan Cheng, Peng Cao, Yixian Liu ✉, Xinya Yuan, Xinyue Zhang, and Haitao Li ✉

Institute for Energy Research, School of Chemistry and Chemical Engineering, Jiangsu University, Zhenjiang 212013, China

Cite this article: *Nano Research*, **2025**, *18*, 94907014. https://doi.org/10.26599/NR.2025.94907014

ABSTRACT: Electrocatalytic chemical oxidation (ECO) is an energy-efficient anodic reaction alternative to the oxygen evolution reaction (OER). ECO lowers the reaction potential and yields higher-value fine chemicals at the anode. The catalyst material plays a crucial role in influencing and determining ECO performance. Enhancing catalyst performance encompasses aspects such as activity, stability, selectivity and cost. Nickel-based electrocatalysts have garnered significant attention for their exceptional performance and widespread use in ECO applications. By modifying nickel-based electrocatalysts, the formation of NiOOH active centers can be encouraged. Strategies such as adjusting size and morphology, doping, introducing defects and constructing heterojunctions are advantageous for enhancing performance. Given the rapid advancements in related research fields, it is imperative to comprehend the mechanisms of nickel-based electrocatalysts in ECO and develop innovative catalysts. This article provides an overview of the modification strategies of nickel-based electrocatalysts, as well as their applications and mechanisms in ECO.

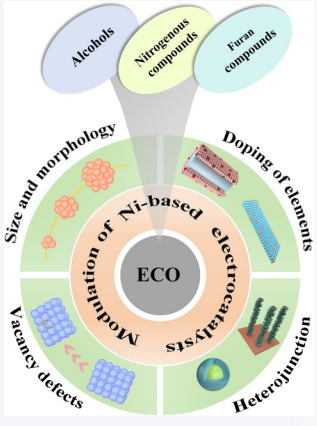

KEYWORDS: anodic reactions, electrocatalytic chemical oxidation, nickel-based electrocatalysts, NiOOH, modification strategies

1 Introduction

The worldwide focus on addressing energy and environmental challenges has made the development of new energy sources a crucial current topic. Hydrogen, as a widely available clean energy, can be efficiently produced through electrocatalytic water decomposition [1–4]. Conventional total water decomposition is an anodic oxygen evolution reaction (OER) coupled with a cathodic hydrogen evolution reaction (HER) [5, 6]. However, OER involves a complex four-electron transfer process with an electrodynamic potential E^{θ} = 1.23 V vs. reversible hydrogen electrode (RHE) [7–9]. The slow kinetic reaction limits the efficiency of the total water decomposition unit [10]. This challenge can be effectively addressed by incorporating urea, alcohol, 5-hydroxymethylfurfural (HMF), hydrazine and other chemicals into the electrolyte to create hybrid water electrolysis [11]. Electrocatalytic chemical oxidation (ECO) can occur at lower potentials, offering an alternative to OER, lowering the reaction potential and yielding higher-value fine chemical products in an environmentally friendly and energy-efficient manner. As to how to improve the performance of anodic chemicals oxidation coupled with cathodic hydrogen precipitation, the design of electrochemical catalysts with excellent performance is the crux [12, 13].

Noble metals (Au, Pt, etc.) have superior adsorption performance for substrates [14], but their scarcity and susceptibility to toxicity limit applications. The modification of catalysts must consider economic cost, catalytic activity, stability and selectivity to determine their suitability for industrial production [15]. To overcome the scarcity of noble metals, the abundance of non-noble transition-metal-based catalysts on the earth has been extensively explored as alternative catalysts [16]. Furthermore, transition-metal-based materials stand out for their superior resistance to toxicity and stability.

Specifically, nickel is a transition metal abundant in the earth's crust. Nickel and its oxides or hydroxides have strong corrosion resistance in alkalinity and are widely used as electrode materials in electrochemical catalysis. Many nickel (Ni)-based catalysts, such as nanocrystalline Ni, $Ni(OH)_2$ nanoribbons, NiO nanosheets (NS), Pt-Ni alloys, have been reported to have good catalytic activity and high toxicity resistance. It is noteworthy that nickel oxides or hydroxides first appear on the surface of Ni-based catalytic

Received: July 15, 2024; **Revised:** August 11, 2024
Accepted: August 29, 2024

✉Address correspondence to Naiyun Liu, liuny@ujs.edu.cn; Yixian Liu, lucien_xian@163.com; Haitao Li, liht@ujs.edu.cn

materials as the potential increases under alkaline conditions. Subsequently, its surface is covered by NiOOH at higher potentials (the potentials under oxidation of anodic chemicals studied in this paper). Promoting the formation of NiOOH may favor the oxidation reaction in several previous studies. Taitt et al. demonstrated the better catalytic activity of NiOOH in electrocatalytic 5-hydroxymethylfurfural oxidation compared to FeOOH and CoOOH. The CoOOH-catalyzed 5-hydroxymethylfurfural oxidation rate was too slow to generate sufficient HMF oxidation current density. And increasing the potential led to the occurrence of OER, which reduced the Faraday efficiency (FE). FeOOH was not even catalytically active in HMF oxidation until an increase in the potential to OER occurred [17]. Therefore, the activity of Ni-based catalysts may have its unique advantages in the field of ECO. Based on the above outstanding advantages, Ni-based catalysts have been deeply studied in this field and have a desirable application prospect.

Different from traditional water electrolysis, hybrid water electrolysis has the problem of anodic OER competing with ECO. It is necessary to minimize the occurrence of OER to reduce energy consumption and improve the efficiency of anodic organics oxidation. Furthermore, chemicals that are predominantly organics produce a wide range of intermediates during oxidation. Therefore, the selectivity of catalysts is a necessary factor to be considered in the design process. In addition, the production of high-value-added fine chemicals by electrocatalytic oxidation of chemicals is indeed energy-efficient and environmentally friendly compared to conventional industrial methods. However, catalysts with excellent stability are required to bring them into large-scale production and life. Consequently, the designed Ni-based catalysts should be capable of reaching the current densities for industrial production at low potentials and have promising selectivity and stability at this potential [18]. A timeline of the recent advances and the modification strategies in the development and utilization of Ni-based materials in ECO is summarized in Fig. 1, including morphology control, defects introduction, heterojunction construction, etc [19–25]. Even though numerous significant research findings have been achieved, the fundamental comprehension of Ni-based electrode materials is still at an early stage of development. Therefore, this paper summarizes the most recent research advancements in electrodes based on Ni-based materials in recent years and predicts their broad application in the field of ECO.

This paper reviews the current research scope of readily oxidizing chemicals used to replace anodic OER. Chemicals are mainly distributed in alcohols, nitrogenous compounds and furan compounds. Additionally, this paper discusses the modification methods of Ni-based catalysts in this field to upgrade their catalytic activity, selectivity and stability. The design strategies of Ni-based catalysts are reviewed in terms of size and morphology control, defects introduction and heterojunction construction (Fig. 2). It will inform the selection of suitable chemicals for the anodic reaction and the design of Ni-based catalysts to achieve the reaction effect.

2 Substrate classification for hybrid water electrolysis

2.1 Electrooxidation of alcohols

Alcohols are electrochemically catalyzed to produce fine chemicals with higher added value in a green and environmentally friendly way [26, 27]. Applications of electrocatalytic alcohol oxidation include fuel cells, biomass utilization and fine chemical synthesis [28]. Nickel hydroxide is characterized by low cost, high catalytic

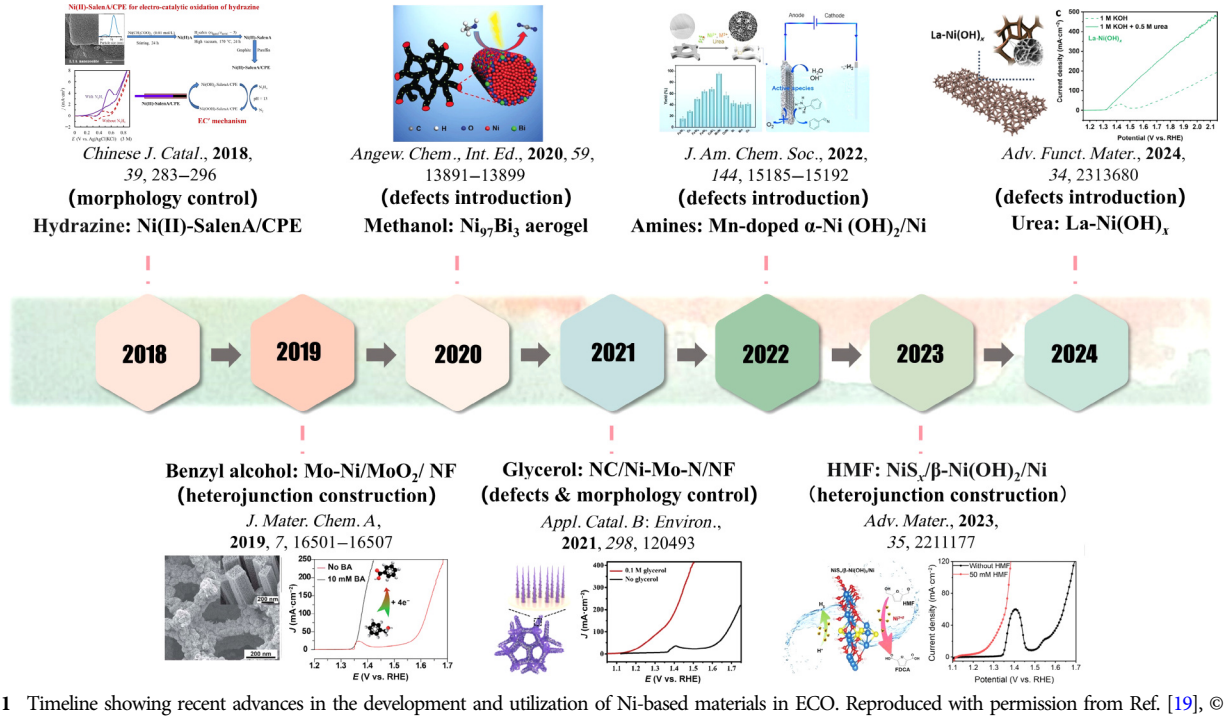

Figure 1 Timeline showing recent advances in the development and utilization of Ni-based materials in ECO. Reproduced with permission from Ref. [19], © Dalian Institute of Chemical Physics, the Chinese Academy of Sciences 2018. Reproduced with permission from Ref. [20], © Wiley-VCH GmbH 2023. Reproduced with permission from Ref. [21], © Wiley-VCH GmbH 2023. Reproduced with permission from Ref. [22], © Wiley-VCH Verlag GmbH & Co. KGaA, Weinheim 2020. Reproduced with permission from Ref. [23], © Elsevier B.V. 2021. Reproduced with permission from Ref. [24], © American Chemical Society 2022. Reproduced with permission from Ref. [25], © The Royal Society of Chemistry 2019.

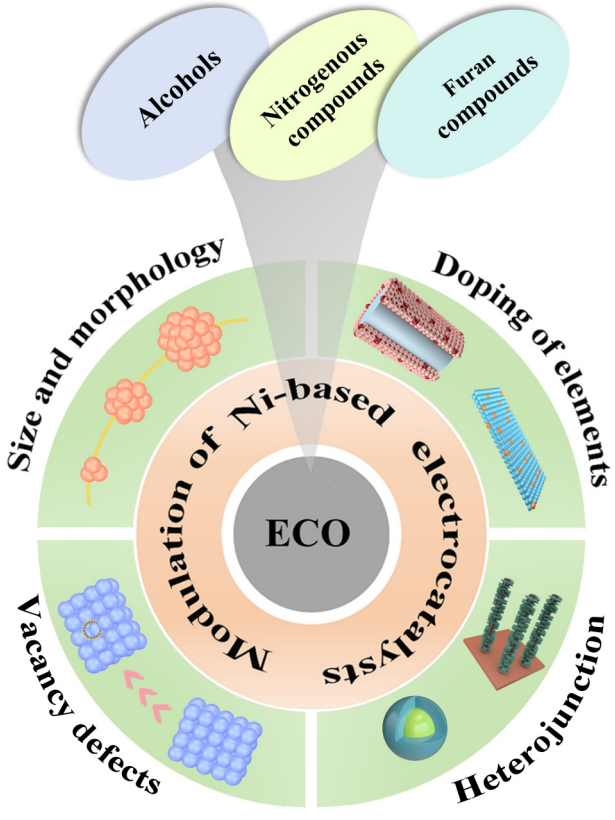

Figure 2 Schematic illustration of the classification of hybrid water electrolysis and modification methods for Ni-based catalysts.

activity and good stability. Therefore, it is a prospective electrocatalyst for the selective oxidation of alcohols to carboxylic acids. The mechanism of alcohol oxidation on nickel hydroxide is the basis for optimizing catalyst performance [29]. The electrocatalytic conversion of alcohols follows two main mechanisms (Figs. 3(a) and 3(b)). Fleischmann's mechanism (indirect oxidation) [30]: nickel hydroxide and nickel oxyhydroxide were used as redox carriers. Once formed, nickel oxyhydroxide directly reacts with alcohols and returns to the initial reaction state of nickel hydroxide. This process couples the oxidation of alcohols with the oxidation of the Ni^{2+}/Ni^{3+} electrical pair. Choi and Hammes-Schiffer et al. on the other hand proposed a hydride transfer mechanism (potential-dependent (PD) oxidation) with Ni^{4+} as the active site. The substrate is transformed in the form of H-transfer through the formation of reactive Ni^{4+}, thus showing a dependence on electric potential [31, 32].

According to Fig. 3(c), aromaticity may enhance the ability of alcohols and aldehydes to undergo oxidation through the indirect oxidation pathway. It could be assigned to the additional stabilization of the radical intermediates which are formed in the indirect pathway, since the radicals formed on C attached to the hydroxyl group (α-C) will be off-domain throughout the adjacent aromatic ring [33, 34]. Thus, aromatic alcohols are more susceptible to indirect oxidation than aliphatic alcohols. Studying the oxidation pathways of alcohols on Ni-based catalytic materials by means of *in situ* Raman spectroscopy and theoretical calculations can help to optimize the catalysts as well as to study the potential dependence.

2.1.1 *Electrooxidation of monohydric alcohols*

Formic acid is a crucial industrial raw material. Obtaining formic

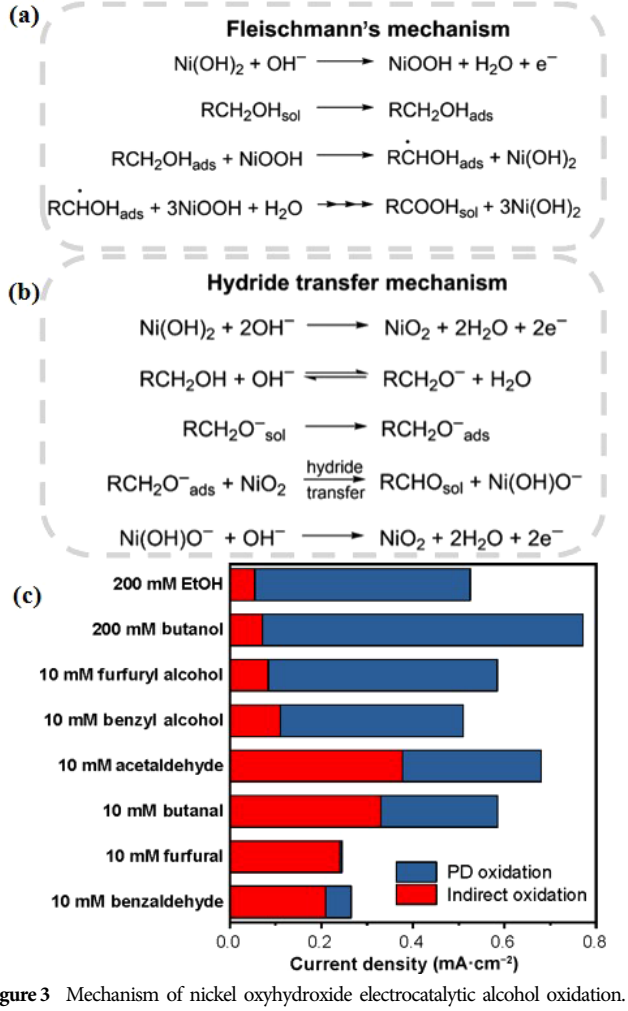

Figure 3 Mechanism of nickel oxyhydroxide electrocatalytic alcohol oxidation. (a) Fleischmann's mechanism. (b) The hydride transfer mechanism. Reproduced with permission from Ref. [34], © American Chemical Society 2023. (c) Component of the current due to Fleischmann's mechanism (indirect oxidation) (red) and hydride transfer mechanism (PD oxidation) (blue) of alcohols and aldehydes at 0.55 V vs. Ag/AgCl and pH 13. Reproduced with permission from Ref. [33], © American Chemical Society 2020.

acid by electrochemical oxidation of methanol is more environmentally friendly and energy efficient. Ni-based catalysts are extensively used in the electrocatalytic methanol oxidation reaction (MOR). Zhu et al. have investigated the structural evolution and reaction mechanism of NiM-layered double hydroxide (LDH) (M = Fe, Mn) catalysts in the MOR for formic acid by employing *in situ* Raman spectroscopy, H/D isotope effect studies and density functional theory (DFT) calculations [35]. They suggested a synergistic or bifunctional catalytic mechanism involving catalytically active sites comprising Ni^{3+} and neighboring electrophilic oxygen species. In this mechanism, Ni^{3+} provides adsorption sites for the reaction substrates and intermediates, while the adjacent electrophilic oxygen sites act as hydrogen acceptors. This facilitates hydrogen transfer between the reaction substrate and the catalyst, leading to the reduction of *in situ* NiOOH to $Ni(OH)_2$ (Figs. 4(a) and 4(b)). This mechanism effectively explains the spontaneous and non-spontaneous MOR processes.

Benzoic acid is typically produced on an industrial scale by oxidizing toluene at high temperatures and pressures, using toxic chemicals. Huang et al. described a more environmentally friendly

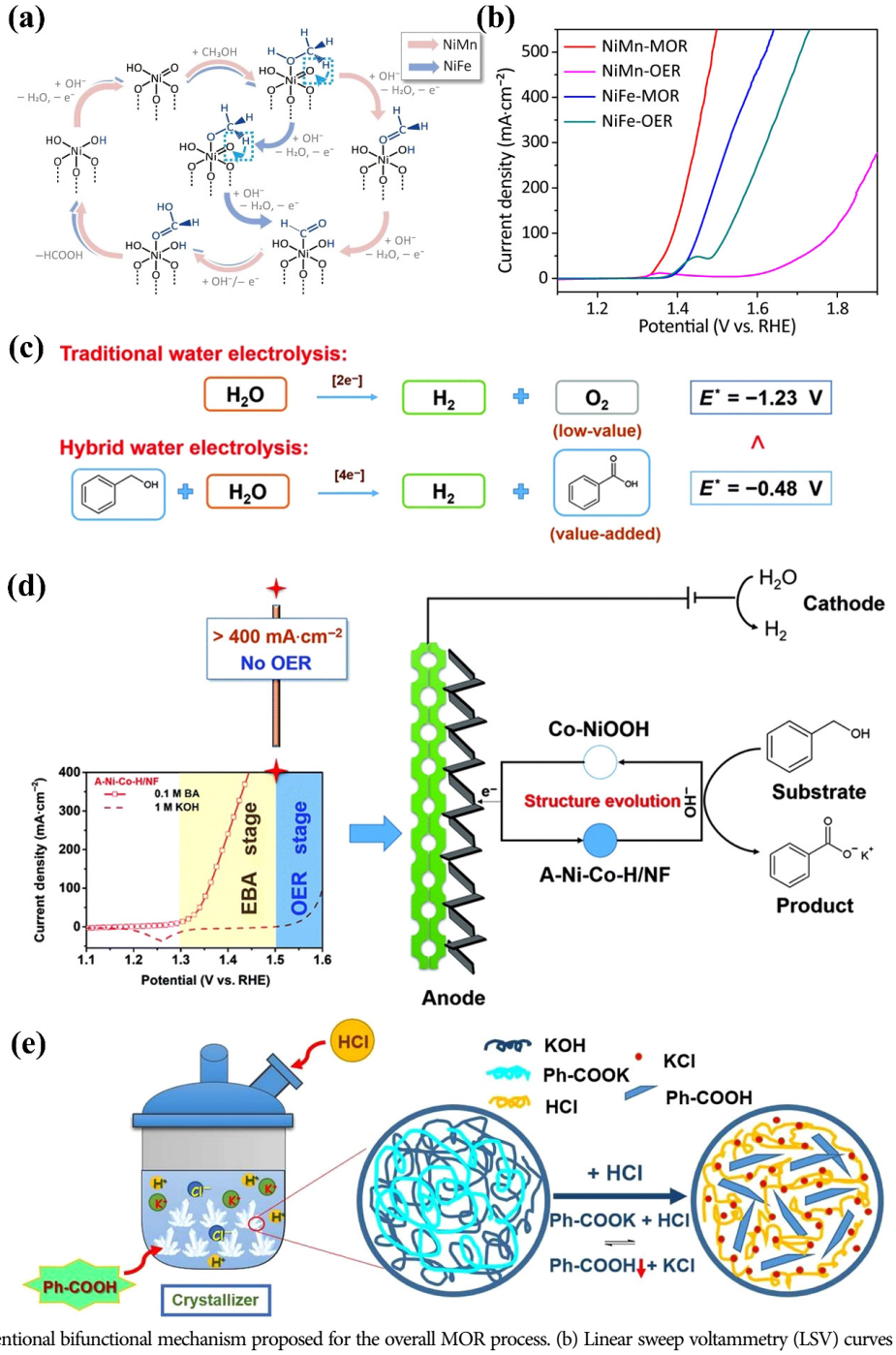

Figure 4 (a) An unconventional bifunctional mechanism proposed for the overall MOR process. (b) Linear sweep voltammetry (LSV) curves of NiMn and NiFe-LDHs were both recorded in 1 M KOH without and with 3 M CH_3OH. Reproduced with permission from Ref. [35], © Zhu, B. T. et al. 2023. (c) The related reactions of traditional water electrolysis and hybrid water electrolysis. (d) Electrocatalytic H_2 generation combined with the production of high-purity Ph-COOH. (e) The diagram of crystallization operation for collecting the electrocatalytic products. Reproduced with permission from Ref. [36], © The Royal Society of Chemistry 2020.

method, which involves using A-Ni-Co-H/NF as a catalyst for the electrochemical oxidation in a benzyl alcohol-containing electrolyte to obtain highly selective benzoic acid products [36]. This Ni-based catalytic material can overcome the competing reaction OER of electrocatalytic benzyl alcohol oxidation reaction (EBA). At an industrial current density of more than 300 $mA·cm^{-2}$, the oxidation of benzyl alcohol was selectively catalyzed to produce high-purity target product benzoic acid at the anode with a yield of close to 100% (Figs. 4(c) and 4(d)). This is a significant breakthrough for the industrial electrocatalytic production of benzoic acid. For the separation of the product, high-purity benzoic acid can typically be obtained by first acidifying the alkaline electrolyte and then using crystallization and separation techniques (Fig. 4(e)). The comprehensive electrochemical production method holds substantial importance for benzoic acid manufacturing.

Monohydric alcohols have only one hydroxyl group, so their adsorption and dehydrogenation processes are relatively simple to operate and involve few intermediate products. Therefore, the product selectivity produced by the method of electrocatalysis has a considerable advantage and is valuable for industrial applications.

2.1.2 *Electrooxidation of polyols*

During the production of biodiesel, a significant amount of glycerol (GLY) by-products is generated, surpassing the current demand [37]. Glycerol is considered an underutilized biomass resource that can be used as a low-cost raw material for industrial production. One potential way to increase its value is through electrocatalytic glycerol oxidation, which can produce higher-value products compared to glycerol itself [38]. Unlike monohydric alcohols, the ease of C–C bond breaking in polyols affects product selectivity. Luo et al. demonstrated the use of a solvothermal preparation method to create PtNi bimetallic nanoparticle (NP) electrocatalysts [39]. When the researchers analyzed the ratio of the two metals, they discovered that the Ni content was consistent throughout the homogeneous alloy. The structure of the PtNi catalyst played a critical role in the C–C bond-breaking ability. Higher Ni content promoted partial C–C bond breaking to produce ethanoic acid and formate, while a more uniformly distributed Pt-Ni promoted the complete oxidation of glycerol to carbonate (Figs. 5(a) and 5(b)). Another study by Li et al. developed a Ni-based catalytic material

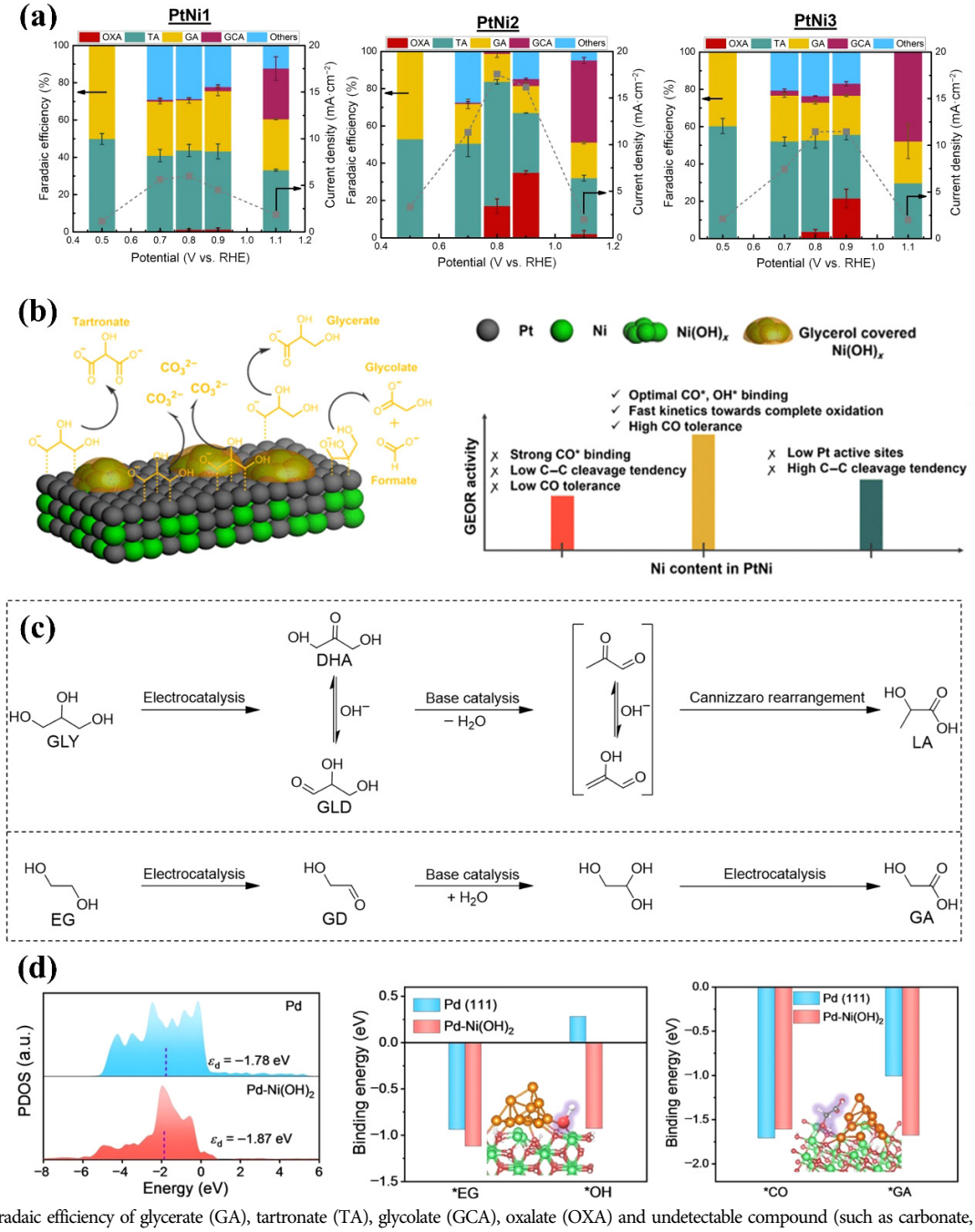

Figure 5 (a) Faradaic efficiency of glycerate (GA), tartronate (TA), glycolate (GCA), oxalate (OXA) and undetectable compound (such as carbonate, formate, etc.) on PtNi1, PtNi2 and PtNi3 at 0.5, 0.7, 0.8, 0.9 and 1.1 V vs. RHE. (b) Illustration of the electronic effect in PtNi electrocatalysts. Reproduced with permission from Ref. [39], © Luo, H. et al. 2022. (c) Proposed reaction mechanisms for electrooxidation of GLY-to-LA (top) and EG-to-GA (down). Reproduced with permission from Ref. [42], © American Chemical Society 2023. (d) Partial density of state (PDOS, d-band) of Pd and Pd-Ni(OH)$_2$, calculated adsorption energies of EG and OH on the surfaces of Pd and Pd-Ni(OH)$_2$ and calculated adsorption energies of GA and CO on the surfaces of Pd and Pd-Ni(OH)$_2$. Reproduced with permission from Ref. [43], © Wiley-VCH GmbH 2023.

composed of amorphous phase nickel hydroxide composite with crystalline phase alkaline copper nitrate [40]. The composite material exhibited different electrochemical reconfigurations at the cathode and anode. It was able to reduce nitrate at the cathode and oxidize glycerol at the anode, resulting in reconstructed materials with potential applications for glycerol oxidation. This work has inspired the future design of dual-functional catalysts.

Waste polyethylene terephthalate (PET) plastic is converted into its monomer glycol, while glycol can be oxidized into high-value-added chemicals by electrocatalytic oxidation. This can effectively alleviate the serious plastic pollution and resource wastage problems faced today [41]. Glycol is very similar to glycerol in that it involves a complex oxidative process and therefore the products are rich and varied. Most of the previous reports occurred with C–C bond breakage ultimately producing C1 products (e.g., formic acid). Yan et al. reported that Au/Ni(OH)$_2$ acted as a catalyst to catalyze the oxidation of both glycerol and ethylene glycol (EG), producing two C2 products, lactic acid (LA) and glycolic acid, respectively (Fig. 5(c)). High current density, high Faraday efficiency and high product selectivity were achieved simultaneously under catalytic conditions [42]. Liu et al. synthesized Pd-Ni(OH)$_2$ composite electrocatalysts. This composite catalyst has high catalytic activity, good stability and excellent selectivity for C2 products. Among them, Ni(OH)$_2$ promoted the generation of OH* active species. OH* facilitated the oxidation of ethylene glycol to ethanoic acid in addition to the removal of toxic carbonyl active species (Fig. 5(d)). The synergistic effect of Pd and Ni sites promoted the rapid desorption and transfer of products from the active Pd site to the inactive Ni site, which terminated the oxidation moderately [43].

Consequently, the relative content of Ni and different modifications for Ni-based catalysts affect the products of polyol oxidation. In particular, the relative content of Ni affects the ease of C–C bond breaking. The loading of noble metals also tends to alter the extent to proceed with the oxidation, resulting in different products. It is worth noting that various noble metals also discriminate between the products due to their different electronic properties.

2.2 Electrooxidation of nitrogenous compounds

Ni-based catalysts are widely used in the electrocatalytic oxidation of nitrogenous compounds such as ammonia, urea, amines and hydrazine. These reactions have well-defined reaction products.

2.2.1 Electrooxidation of urea

Urea is found in large quantities in industrial and domestic wastewater. It is easily converted into ammonia, oxides of nitrogen and nitrites, which have a significant impact on human health and the environment. Urea has a high energy density, about ten times that of hydrogen energy. In recent years, Ni-based catalysts for electrocatalytic urea oxidation have been widely studied. Urea is oxidized to produce environmentally non-polluting carbon dioxide and nitrogen with Ni-based catalysts. The formation of N–N bonds by independent nitrogen atoms in urea is an interesting process. Wang et al. proposed the mechanism of electrochemical oxidation of urea with β-Ni(OH)$_2$ catalyst [44]. The first step of catalyst dehydrogenation and oxidation reaction and the second step of urea dehydrogenation and oxidation reaction, respectively (Fig. 6(a)).

However, oxidation of the urea molecule is a six-electron and six-proton transfer process. Moreover, its structure of multiple ligand centers is prone to excessive oxidation of urea to generate toxic and harmful nitrogen oxides. Li et al. investigated the fate of nitrogen in the oxidation of urea by isotope labeling method [45]. A polyaniline-modified electrode that can promote the doubled generation of nitrogen species was invented. It can suppress the formation of over-oxidation products (Fig. 6(b)). This strategy, which is in line with sustainable development, is a great inspiration for the researchers behind.

2.2.2 Electrooxidation of ammonia

Although ammonia can be used as a fertilizer, it can also pollute the environment. Excessive levels of ammonia in water can lead to a reduction in dissolved oxygen and eutrophication of water bodies [46]. Electrocatalytic ammonia oxidation is a beneficial pathway for the nitrogen cycle [47]. However, there is excessive oxidation of ammonia to environmentally unfavorable oxides of nitrogen during ammonia oxidation [48]. In addition, the competitive reaction between ammonia oxidation and OER is also a problem to be considered in the design of catalysts.

Oswin and Salomon proposed a mechanism for the continuous dehydrogenation of ammonia (O–S mechanism). Adsorption of ammonia progressively dehydrogenates to give *N [49, 50] and *N couples to ultimately give N_2 [51]. Gerischer and Maurer proposed another mechanism (G–M mechanism) [52]. Adsorbed ammonia dehydrogenates and then dimerizes to form a hydrazine-like structure, ultimately generating N_2. In the actual ammonia oxidation process, the two mechanisms are competitive (Fig. 7(a)). It has been shown that the O–S mechanism is more likely to be followed at high potentials. However, the G–M mechanism is followed at low potentials [53]. The pH of the electrolyte affects the oxidation peak current density of the ammonia oxidation reaction. The peak current showed a good linear relationship with pH [54]. Allagui et al. concluded that an alkaline environment is necessary for the completion of the reaction by varying the pH of the electrolyte. The current density of the ammonia oxidation peak increased somewhat linearly with pH up to 10.5. In addition, electrooxidation on Ni(OH)$_2$/NiPd was in the un-ionized form of ammonia [55]. Accordingly, regulating the pH of electrolytes along with determining the oxidation mechanism is of significance in practical applications.

2.2.3 Electrooxidation of hydrazine

Electrocatalytic hydrazine oxidation is another common anodic reaction used as an alternative to OER-coupled hydrogen production [56]. The thermodynamic potential for the four-electron transfer hydrazine oxidation ($N_2H_4 + 4OH^- \rightarrow N_2 + 4H_2O + 4e^-$) is −0.33 V vs. RHE. This is much lower than the potential of OER, making it difficult for mixed O_2 and H_2 production to occur [57–59]. Zhang et al. designed vanadium-doped nickel nitride nanosheet materials for the oxidative coupling of hydrazine to hydrogen precipitation. It was shown that among the different conformations of hydrazine adsorbed on the catalyst surface, the trans conformation was the most favorable one for adsorption (Fig. 7(b)). Moreover, vanadium doping promoted the dehydrogenation process of hydrazine, resulting in higher catalytic activity [60]. Xu et al. developed NiRh-BDC catalysts (BDC: 1,4-benzenedicarboxylate ligands) by introducing the noble metal Rh into Ni-based metal-organic framework (MOF). The Ni site adjacent to Rh transfers electrons to Rh, thus lowering the energy barrier for hydrazine dehydrogenation at the Ni site [61]. Therefore, there is no carbon emission during the oxidation of hydrazine and nitrogen as its sole product does not pose a hazard when mixed with hydrogen. Its

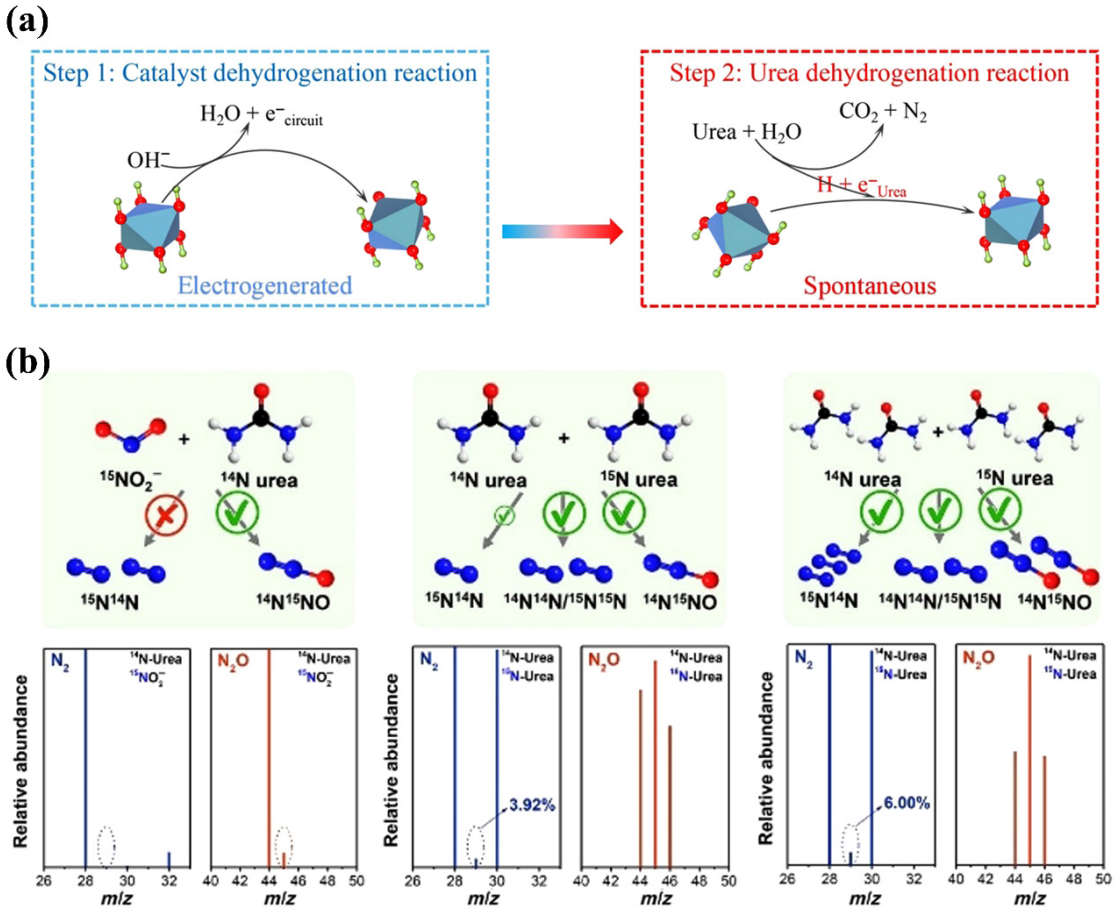

Figure 6 (a) The UOR mechanism on the β-Ni(OH)$_2$ electrode. Reproduced with permission from Ref. [44], © Wiley-VCH GmbH 2020. (b) The mass spectrometry (MS) spectra of the gaseous products during UOR with $^{15}NO_2^-$ pre-added 0.33 M ^{14}N-urea, 0.33 M ^{14}N-urea and ^{15}N-urea mixture and 1.00 M ^{14}N-urea and ^{15}N-urea mixture (molar ratio = 1:1) in 1 M KOH. Reproduced with permission from Ref. [45], © Wiley-VCH GmbH 2021.

superior overpotential avoids OER competition and is a promising alternative reaction to OER.

2.2.4 *Electrooxidation of amines*

Electrocatalytic selective oxidation of amines to nitriles is a value-added reaction of amines. Nitrile is commonly used as an intermediate in paints, pesticides and certain organic products. It is an important raw material for organic synthesis [62, 63]. Conventional methods for the synthesis of nitrile include the nitrification of alkyl halides and the oxidation of ammonia or amines at high temperatures and under strong oxidant conditions. In contrast, electrocatalytic amine oxidation is more energy-efficient, green and environmentally friendly. Ding et al. synthesized Ni_2P nanosheets grown on nickel foam (NF) to highly selectively oxidize benzylamine to benzonitrile [64]. Sun et al. found that Mn-doped α-Ni(OH)$_2$ has good catalytic activity in the electrocatalytic oxidation of amines to nitriles. Moreover, the researchers proposed a dual adsorption mechanism for OER and amine oxidation intermediates (Fig. 7(c)). Mn and Ni promoted the adsorption of amine and active oxidation intermediates on the catalysts, respectively [24]. The proposed dual adsorption mechanism offers a reference for using catalysts based on the OER reaction to oxidize related chemicals.

2.3 Electrooxidation of furan compounds

The electrocatalytic oxidation of furfuryl alcohol, furfural and 5-hydroxymethylfurfural from furan compounds has also been extensively studied. This group of organics can be obtained from biomass. In most cases, electrocatalytic oxidation of furfuryl alcohol yields furfural or furoic acid. Moreover, the electrocatalytic oxidation of furfural and 5-hydroxymethylfurfural yields furoic acid and 2,5-furandicarboxylic acid (FDCA), respectively.

2.3.1 *Electrooxidation of furfuryl alcohol and furfural*

Furfuryl alcohol is cheap in the market. Moreover, furfuryl alcohol does not spontaneously undergo the Cannizzaro reaction. Furfural is produced primarily by hydrolysis and dehydration of xylose [65]. Furoic acid is more than three times as expensive as furfural. Therefore, obtaining furoic acid by electrocatalytic oxidation of furfuryl alcohol or furfural is a value-added reaction and can be used as an alternative to OER. Three-dimensional (3D) layered nickel-iron micro-flowers catalysts synthesized by electrodeposition method were used for electrocatalytic furfuryl alcohol oxidation to produce furoic acid by Liu et al. Furfuryl oxidation showed a lower overpotential than OER in the catalyzed reaction. The conversion of furfuryl alcohol was 81.3% and the selectivity of furoic acid was 94% after 3 h of catalytic reaction [66]. Fang et al. applied different potentials to the catalyst to oxidize furfuryl alcohol to furfural and furoic acid, respectively. And furfural was used as an intermediate for the oxidation of furfuryl alcohol to furoic acid (Fig. 8(a)) [67]. Lu et al. investigated the performance of the electrooxidation of the substrates furfuryl alcohol and furfural over the designed β-

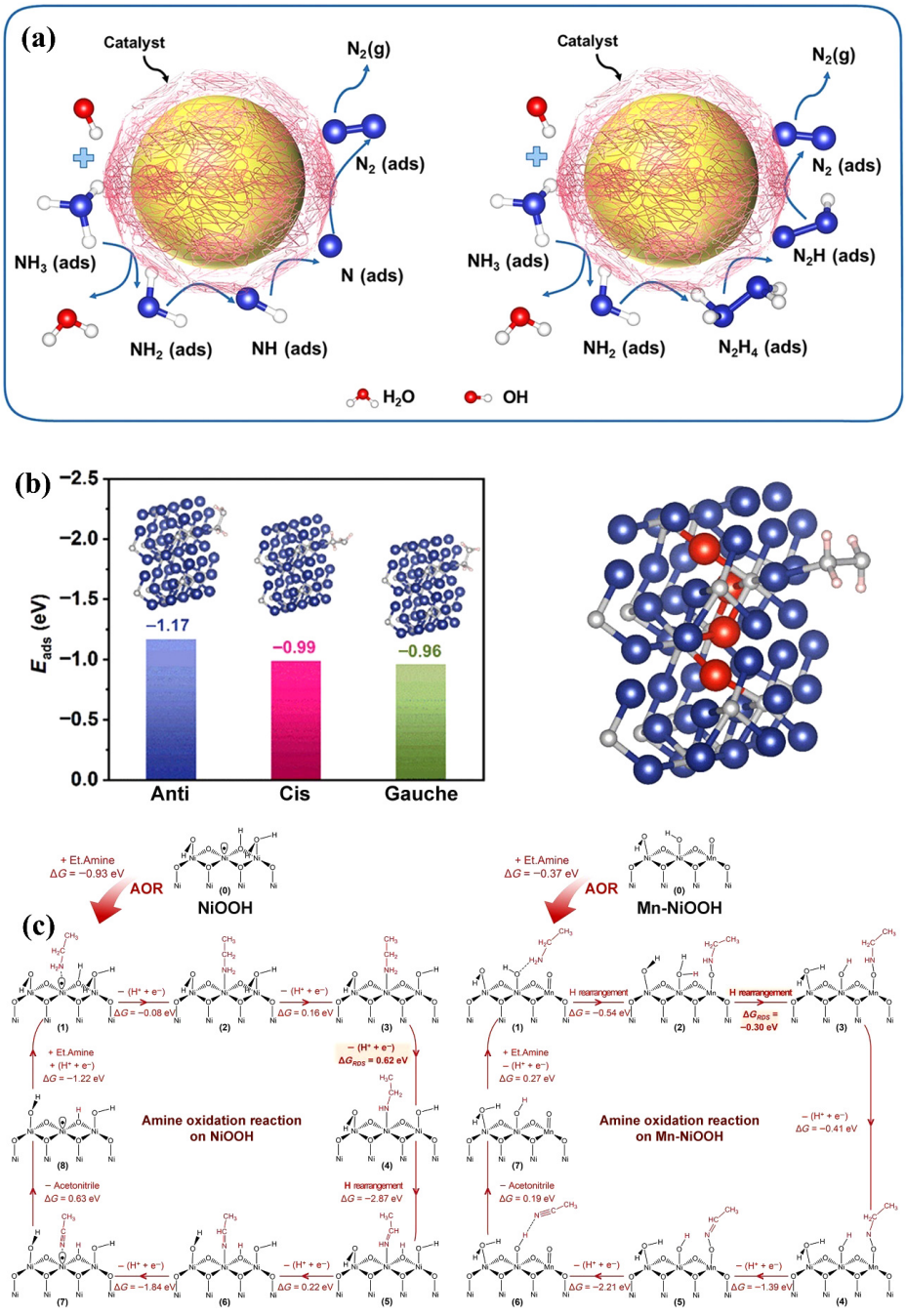

Figure 7 (a) Ammonia oxidation upon O–S and G–M mechanism. Reproduced with permission from Ref. [53], © Tian, Y. R. et al. 2023. (b) Different adsorption configurations of the N_2H_4 molecule on the Ni_3N (001) surface and side-view image of the V-Ni_3N model with an adsorbed N_2H_4 molecule. Reproduced with permission from Ref. [60], © American Chemical Society 2021. (c) Reaction-free energy diagrams for the amine oxidation reaction on NiOOH (left) and Mn-NiOOH (right). Reproduced with permission from Ref. [24], © American Chemical Society 2022.

$Co_{0.1}Ni_{0.9}(OH)_2$ catalyst. The characteristic groups of furfuryl alcohol and furfural were hydroxyl and aldehyde groups, respectively. The results of the study showed that the oxidation performance of furfural was better than that of furfuryl alcohol [68].

Consequently, the aldehyde group may be more susceptible to oxidation than the hydroxyl group, which informs the oxidation pathway of 5-hydroxymethylfurfural as well as the selectivity of alcohol oxidation.

2.3.2 *Electrooxidation of 5-hydroxymethylfurfural*

The reaction history of the oxidation of 5-hydroxymethylfurfural is shown in Fig. 8(b) [69]. The final 2,5-furandicarboxylic acid is a very widely used organic compound. Polyethylene 2,5-furandicarboxylate can be generated from 2,5-furandicarboxylic acid. It has a similar conjugated carbocyclic ring and dicarboxylic acid structure to petroleum-based terephthalic acid [70]. In addition, polyethylene 2,5-furandicarboxylate has good thermal stability compared to polyethylene terephthalate generated from petroleum-based terephthalic acid [71–73].

5-Hydroxymethylfurfural contains both hydroxyl and aldehyde groups. Therefore, the order of oxidation of the functional groups is important for probing the mechanism of 5-hydroxymethylfurfural

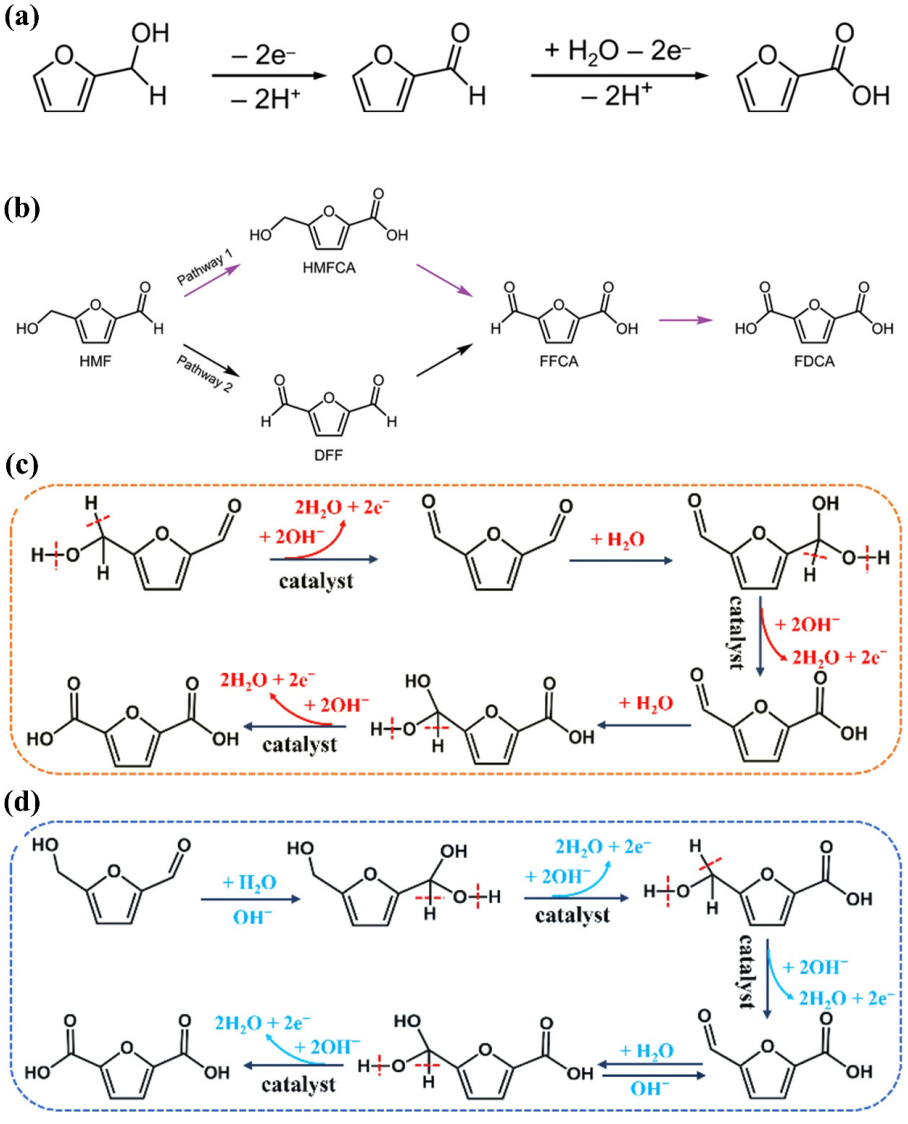

Figure 8 (a) Possible oxidation pathway from furfuryl alcohol to 2-furoic acid. Reproduced with permission from Ref. [67], © American Chemical Society 2021. (b) Two possible pathways for the oxidation of 5-hydroxymethylfurfural to 2,5-furandicarboxylic acid. Reproduced with permission from Ref. [69], © Wiley-VCH GmbH 2023. Possible reaction mechanism for the electrocatalytic generation of 2,5-furandicarboxylic acid from HMF at (c) non-strong alkali electrolyte (pH < 13) and (d) strong alkali electrolyte (pH ≥ 13), the OH^- below the arrow indicates the reaction condition under alkaline catalysis. Reproduced with permission from Ref. [74], © Jiang, X. L. et al. 2023.

oxidation reactions involving 6-electron transfer. Jiang et al. showed that the hydroxyl group can be oxidized before the aldehyde group when the pH is less than 13 (Fig. 8(c)). When the pH value is above 13 (Fig. 8(d)), the aldehyde group is oxidized first [74]. Ni-based catalytic materials have been widely used in electrocatalytic oxidation of 5-hydroxymethylfurfural. However, the activity of 5-hydroxymethylfurfural electrocatalytic oxidation is not high due to the poor adsorption ability of 5-hydroxymethylfurfural and hydroxyl radicals on Ni-based materials. Wu et al. demonstrated the role of Pt in regulating the oxidation of Ni in the prepared Pt_xNi_{100-x} nanowire (NW) catalytic materials [75]. Pt and Ni formed a Pt–O–Ni bond in which Pt promoted the adsorption of hydroxyl radicals on Ni. While the interaction between Ni and Pt electrons promoted the adsorption of 5-hydroxymethylfurfural on the materials. Synergistic interaction between Ni and Pt promoted the formation of NiOOH activity center formation, resulting in a substantial increase in the activity of the 5-hydroxymethylfurfural oxidation reaction. The hydroxyl group is oxidized before the aldehyde group when the pH is below 13, while the aldehyde group is oxidized first when the pH is above 13. Based on this fact, the effect of pH on selectivity compelled to be considered in the study. In addition, enhancing the adsorption capacity of 5-hydroxymethylfurfural on Ni-based catalysts can significantly promote the oxidation reaction.

3 Design strategies for Ni-based catalysts

ECO has high requirements for catalyst activity, selectivity and stability. Therefore, the design of suitable catalysts is the key to the study of ECO. In recent years, researchers have designed a variety of catalysts for ECO and the proportion of Ni-based catalysts should not be neglected. Table 1 exhibits the comparison of the activity of various Ni-based catalysts in different hybrid water electrolysis. The state of Ni-based catalysts under alkaline conditions is to reconfigure from nickel hydroxide or oxide to NiOOH with the increase of potential. The substrate is

Table 1 The activity of various Ni-based catalysts in different hybrid water electrolysis

Catalyst	Substrate	Electrolyte	Modification strategies	Potential (V vs. RHE)@ current density ($mA·cm^{-2}$)	References
NiMn-LDH	Methanol	1 M KOH + 3 M substrate	Defects	1.4@100	[36]
A-Ni-Co-H/NF	Benzyl alcohol	1 M KOH + 0.1 M substrate	Defects	1.35@100	[35]
Au/$Ni(OH)_2$	Glycerol	3 M KOH + 0.3 M substrate	Heterojunction	0.95@317.7	[42]
Pd-$Ni(OH)_2$	Ethylene glycol	1 M KOH + 1 M substrate	Heterojunction	0.69@100	[43]
B-$Ni(OH)_2$	Urea	1 M KOH + 0.05 M substrate	Morphology	1.5@5	[45]
$NiMoO_4$	Urea	1 M KOH + 0.33 M substrate	Morphology	1.5@50	[44]
V-Ni_3N NS	Hydrazine	1 M KOH + 0.1 M substrate	Defects	0.05@100	[60]
$NiRh_{0.016}$-BDC	Hydrazine	1 M KOH + 0.3 M substrate	Defects	0.1@300	[61]
Ultrathin Ni_2P nanomeshes on NF (Ni_2P-UNMs/NF)	Benzylamine	1 M KOH + 0.125 M substrate	Defects	1.5@80	[64]
Mn-α-$Ni(OH)_2$	Benzylamine	1 M KOH + 0.025 M substrate	Defects	1.4@20	[19]
NiFe	Furfuryl alcohol	1 M KOH + 0.001 M substrate	Defects	1.6@40	[66]
B-$Co_{0.1}Ni_{0.9}(OH)_2$	HMF	1 M KOH + 0.05 M substrate	Defects	1.6@9	[68]
$Pt_{26}Ni_{74}$ NWs	HMF	1 M KOH + 0.05 M substrate	Defects and morphology	1.5@70	[75]

subsequently oxidized by NiOOH to generate a sequence of value-added chemicals, while NiOOH is reduced to $Ni(OH)_2$. The process is repeated at a high potential where it is oxidized again to NiOOH. Due to the complexity of the substrate reaction steps and the variety of intermediates, the NiOOH sites are easily occupied by intermediates and are poisoned and deactivated, preventing further catalytic regeneration. Accordingly, the main lines of thought in designing catalysts are (1) to promote the reconstruction of Ni-based catalysts to NiOOH, (2) to foster the exposure of NiOOH active sites and (3) to enhance the intrinsic activity of the catalysts. Modulation of size and morphology may increase the specific surface area and intrinsic activity of the catalysts, thus favoring an enhanced number of NiOOH sites. Doping strategies may be accompanied by vacancies, phase transitions and structural distortions. Heteroatoms enable the displacement of the Fermi energy levels of the catalysts and change the energy band structure of the catalysts. They modulate the electronic structure of the materials and the interactions between the electrons to promote the regeneration of NiOOH sites. The modulation of the electronic structure of the catalyst surface by the vacancy defects affects the coordination environment of the NiOOH sites and its optimization of the free energy of adsorption of substrates and intermediates on the catalyst surface facilitates the reaction of substrates on the catalyst surface. Additionally, the heterojunction can effectively regulate the stability, conductivity and hydrophilicity of the material by rationally combining different components. Therefore, modification of catalysts by these methods can effectively solve the above problems.

3.1 Modulation of catalyst size and morphology

Low-dimensional nanomaterials (zero-dimensional, one-dimensional, two-dimensional and multi-dimensional combinatorial materials) have characteristic dimensions similar to the De Broglie wavelength of an electron. The movement of electrons in the materials is restricted. Their energies are changed from a continuous state to a discontinuous energy level, which in turn gives rise to many new properties [76]. Low-dimensional nanomaterials increase the specific surface area of the catalytic material, which contributes to the exposure of active sites and thus improves the activity of the catalyst. Most of the catalysts for ECO are low-dimensional nanomaterials. Considering that the catalytic reaction occurs on the surface of the catalyst, size modulation (e.g., particle size, thickness, etc.) based on low-dimensional nanomaterials can increase the specific surface area of the catalyst and thus enhance the catalytic activity of the catalyst [77]. Normally, the size of the material is reduced to increase the specific surface area of the material.

Wu et al. demonstrated that the modulation of the catalyst size can change the intrinsic activity of the materials in addition to the specific surface area [78]. Normalizing the catalytic activity gives the intrinsic activity. The results show that adjusting the size can change the surface electronic structure, which affects the adsorption of intermediates. In turn, the reaction pathway changes. Catalysts have the best performance at a certain optimal particle size. The optimal performance usually results from the competitive or cooperative effects of surface area and intrinsic activity. Therefore, the performance of a material can be improved by controlling the particle size and morphology of the catalyst when designing the catalyst.

3.1.1 Zero-dimensional nanomaterials

Common zero-dimensional materials are nanoparticles, nanoclusters (NCs) and quantum dots. They are nanoscale in all three dimensions [79]. Modulating the size of nanomaterials can change the properties of the material [80, 81]. The decrease in the size of nanoparticles leads to geometrical and electronic effects [82]. As the size decreases, the ratio of surface atoms to the total number of atoms increases [83]. At the edges and corners are low-coordinated atoms. Then the size reduction causes the number of low-coordinated atoms to increase, while the number of highly-coordinated atoms is elevated accordingly. The degree of coordination unsaturation of the surface atoms increases accordingly. This leads to a change in the nature of the catalytic reaction carried out by the catalyst. In addition, the energy band

structure of the nanoparticles changes as the particle size decreases. Smaller-sized nanoparticles are closer to molecules in this respect [84].

The effect of nickel nanoparticles of different sizes on the oxidation performance of benzyl alcohol was recently published by Zhong et al. They obtained 1.0, 1.9 and 8.3 nm nickel nanoparticles on nitrogen-doped carbon substrates by reducing Ni^{2+} with hydrogen at different temperatures of 200, 280 and 500 °C, respectively (Fig. 9(a)) [85]. The final results showed that the medium-sized catalytic material showed the best reduction effect at 280 °C (Fig. 9(b)). And the yield of benzoic acid reached 99%, which was higher than that of the small-sized catalytic material (82%) and the large-sized catalytic material (55%). Meanwhile, theoretical calculations showed that the size changed the nature of the surface sites of the materials, which contributed to the change in the adsorption energy of benzyl alcohol on the surface of the materials.

Liu et al. loaded different sizes of noble metal Pd (Pd single atoms (SAs), Pd nanoclusters and Pd nanoparticles) on NiFe-LDH for electrocatalytic hydrazine hydrate oxidation (Fig. 9(c)) [86]. Electrochemical tests revealed that the medium-sized Pd nanocluster-loaded NiFe-LDH had the highest current density at 0.35 V vs. RHE potential. Its mass activity was 36 times higher than that of Pd single-atom loaded NiFe-LDH and 7 times higher than that of Pd nanoparticle-loaded NiFe-LDH. The distance spacing between the catalytic sites in Pd single-atom loaded NiFe-LDH was relatively large and the catalytic sites were independent. The aggregation of the catalytic sites in Pd nanoparticle-loaded NiFe-LDH led to a large site resistance. Whereas, the Pd nanoclusters exhibit stronger intra-cluster interactions and weaker spatial site resistance, leading to hybridization of the Pd d-orbitals with the σ-orbitals of the hydrazine molecules (Fig. 9(d)). Accordingly, zero-dimensional materials may not be as small in size as they could be but rather need to find a balance between spatial site resistance and interatomic interactions.

3.1.2 *One-dimensional nanomaterials*

In addition to zero-dimensional nanomaterials, one-dimensional nanomaterials (nanowires, nanorods, nanotubes, etc.) have also been extensively investigated. One-dimensional nanomaterials shorten ion diffusion channels and promote electron transport [87]. It has a large specific surface area, increasing the contact area between the electrolyte and electrode. The unique solubility resistance of one-dimensional nanomaterials reduces volume changes and thus extends the life of the material [88]. Therefore, one-dimensional nanomaterials have good catalytic properties.

Chen et al. developed Mn-$Ni(OH)_2$ porous nanowire arrays (PNAs) as catalytic materials for urea electrocatalytic oxidation (Fig. 10(a)) [89]. The results showed that the porous nanowire array structure could provide a wide space for plasmonic electron transfer. It promotes the exposure of active sites and enhances the catalytic activity for urea oxidation. The Mn-$Ni(OH)_2$ porous nanowire array catalytic materials exhibit good catalytic activity and stability for urea oxidation (Fig. 10(b)).

Ultrafine Pt-Mo-Ni nanowires with ultrahigh aspect ratio for electrocatalytic alcohol oxidation were synthesized by Mao et al. (Fig. 10(c)). The micrometer length and 2.5 nm diameter resulted in ultrafine nanowire structures with a high ratio of surface atoms to the total number of atoms (Fig. 10(d)) [90]. Pt atoms are noble metals and increasing the efficiency of utilizing Pt atoms can reduce the overall cost of the catalyst. The ultrafine nanowire structure with a high percentage of surface atoms improves the atomic efficiency of Pt. In addition, surface defects are created by Ni and avoiding the aggregation of Pt atoms creates a large spatial barrier and is sufficient to segregate Pt atoms on the surface and create surface defects. Moreover, Ni and Pt atoms are stabilized by Mo. This work is of good significance for the design of catalysts.

Yu et al. loaded rod-shaped Ni-Mo-O on nickel foam by hydrothermal method and calcined it under argon and hydrogen atmosphere as catalysts for urea oxidation and hydrogen

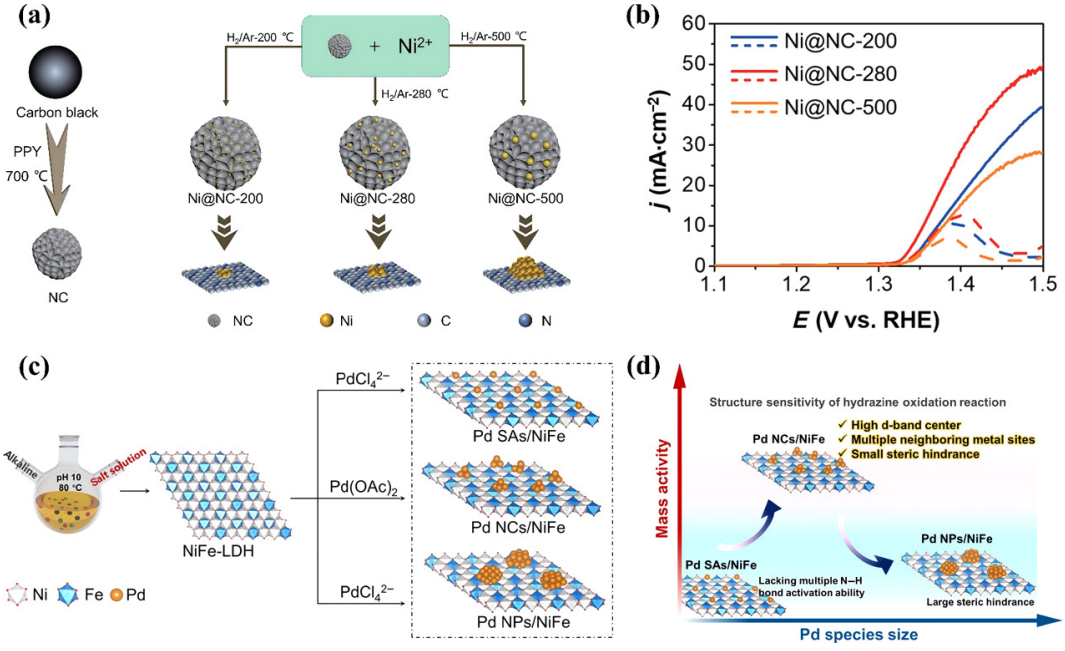

Figure 9 (a) The schematic procedure for the preparation of Ni@NC-200, Ni@NC-280, Ni@NC-500. (b) LSV curves of Ni@NC-200, Ni@NC-280 and Ni@NC-500 in 1.0 M KOH with (solid line) and without (dotted line). Reproduced with permission from Ref. [85], © Tsinghua University Press 2022. (c) Illustration of the preparation of Pd SAs/NiFe, Pd NCs/NiFe and Pd NPs/NiFe. (d) Structural sensitivity schematic of the hydrazine oxidation reaction (HzOR). Reproduced with permission from Ref. [86], © American Chemical Society 2022.

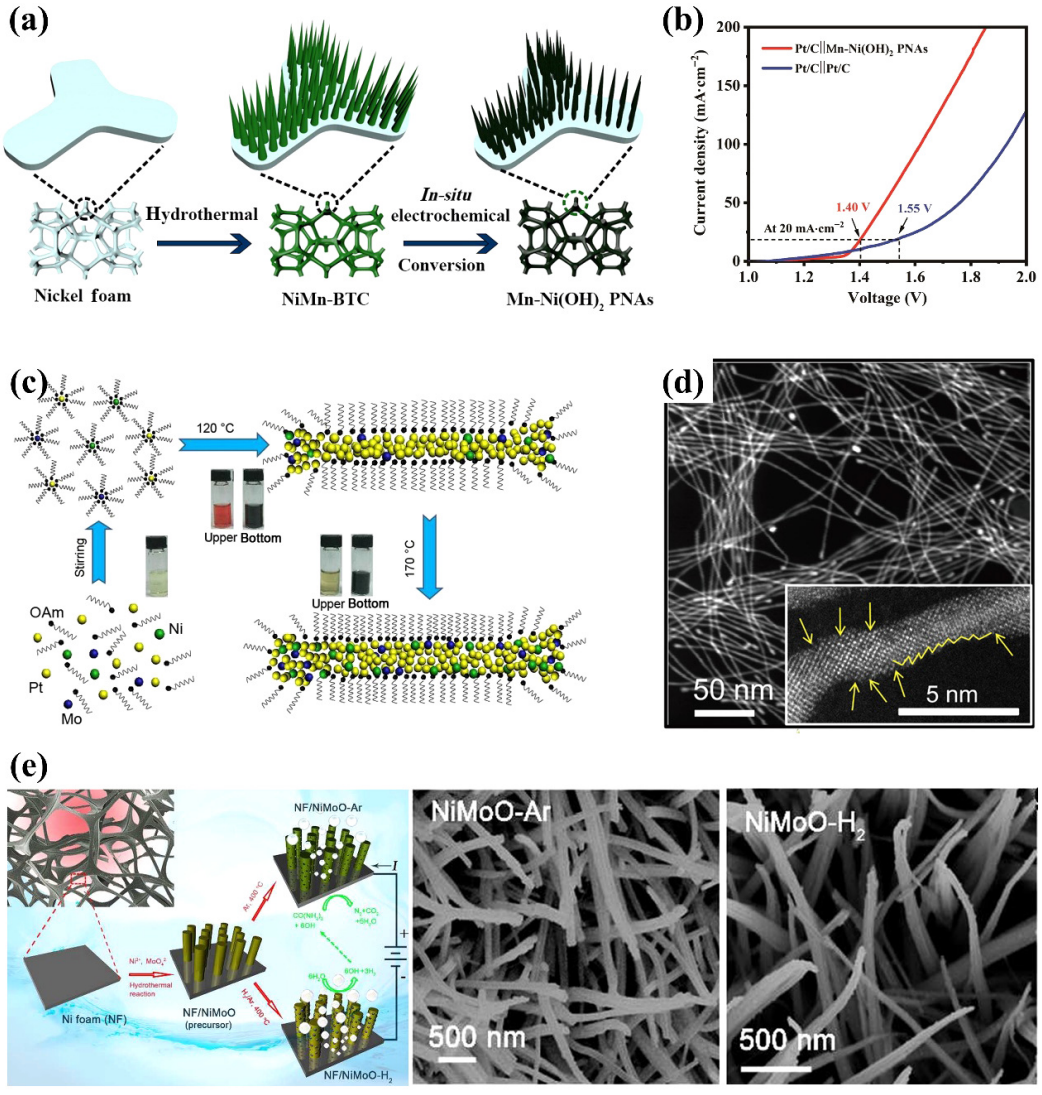

Figure 10 (a) Schematic of the fabrication process of Mn-Ni(OH)$_2$ PNAs. (b) LSV plots of Pt/C||Mn-Ni(OH)$_2$ PNAs and Pt/C||Pt/C two-electrode systems for overall urea electrolysis in an alkaline solution. Reproduced with permission from Ref. [89], © Elsevier Inc. 2022. (c) Schematic of the growth mechanism of the Pt-Mo-Ni NWs. (d) High-angle annular dark-field scanning TEM (HAADF-STEM) image of the Pt-Mo-Ni NWs. Reproduced with permission from Ref. [90], © Mao, J. J. et al. 2017. (e) Schematic illustration of the preparation of NF/NiMoO-Ar as UOR catalyst and NF/NiMoO-H$_2$ as HER catalyst and scanning electron microscopy (SEM) images. Reproduced with permission from Ref. [91], © The Royal Society of Chemistry 2018.

precipitation, respectively (Fig. 10(e)) [91]. The current density of the electrolytic cell consisting of urea oxidation and hydrogen precipitation could reach 10 mA·cm^{-2} at a low potential of 1.38 V vs. RHE.

One-dimensional nanomaterials with ultra-high aspect ratios can provide a wide space for plasmonic electron transfer. In addition, their ultra-high surface atomic ratio improves atomic efficiency. When modified with precious metals, the cost of the material can be effectively reduced.

3.1.3 *Two-dimensional nanomaterials*

Considering two-dimensional nanomaterials with a great specific surface area resulting from a great planar size and atomic thickness, the ratio of the number of surface atoms to the total number of atoms is high [92–94]. The catalytic properties of the materials can be modulated by surface modification. The electrons move only in the two-dimensional planar range and the materials have superior electronic properties [95, 96].

Jiang et al. used a one-step solvothermal method to load two-dimensional nickel organic skeleton nanosheets with different thicknesses on nickel foam (Fig. 11(a)) [97]. The electrochemical test results showed that the catalyst loaded with the thinnest thickness of nanosheets had the best electrocatalytic urea oxidation activity (Fig. 11(b)). The current density of urea oxidation reached 100 mA·cm^{-2} at a low potential of 1.45 V vs. RHE (Fig. 11(c)). The current density of the electrolytic cell for urea oxidation coupled with cathodic hydrogen precipitation reached 50 mA·cm^{-2} at a low potential of 1.53 V vs. RHE (Fig. 11(d)).

Hao et al. synthesized Ni(OH)$_2$ nanosheet arrays *in situ* on nickel foam for methanol oxidation-coupled hydrogen production [98]. A current density of 10 mA·cm^{-2} at a low voltage of 1.52 V was achieved. The methanol oxidation was highly selective to produce formate with higher value, while the H_2 yield was more than 92%. Zhang et al. reported the *in situ* growth of ultrathin nanosheets on a nickel foam surface as an anodic catalyst to catalyze the oxidation of 5-hydroxymethylfurfural to 2,5-furandicarboxylic acid [99]. At a

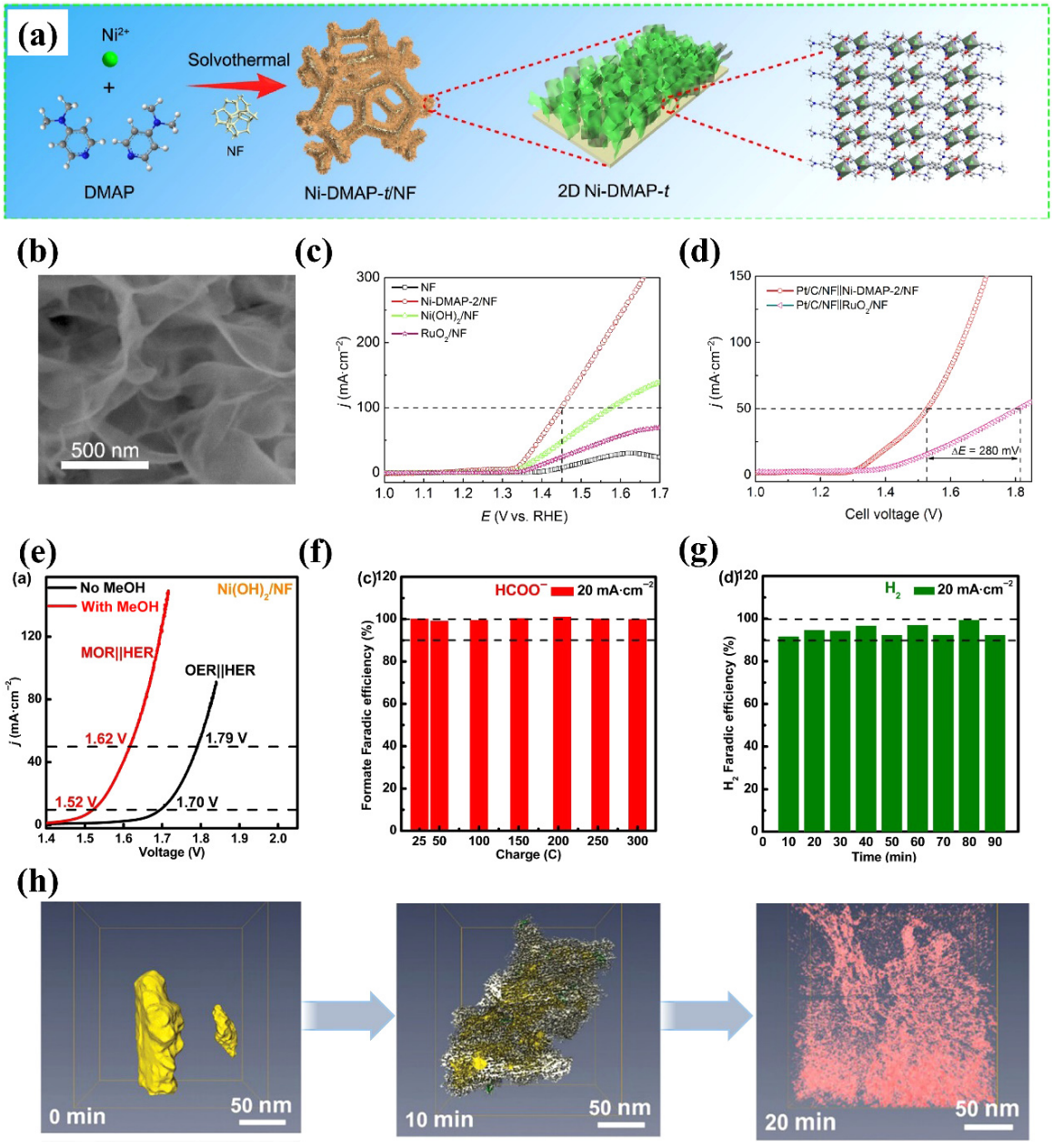

Figure 11 (a) Schematic illustration of the synthesis process of Ni-DMAP-*t*/NF (DMAP-*t*: an organic ligand of 4-dimethylaminopyridine, where *t* is the synthesis time). (b) SEM images of Ni-DMAP-2/carbon cloth (CC). (c) LSV curves of NF, $Ni(OH)_2$/NF, Ni-DMAP-2/NF and RuO_2/NF in 1.0 M KOH + 0.5 M urea. (d) Polarization curves of Pt/C/NF||Ni-DMAP-2/NF and Pt/C/NF||RuO_2/NF coupled electrodes in urea electrolysis. Reproduced with permission from Ref. [97], © Elsevier Ltd. 2022. (e) Cell LSV curve comparison of MOR||HER and overall water splitting (OER||HER) using $Ni(OH)_2$/NF as anode and cathode in 1.0 M KOH with and without 500 mM MeOH. (f) The FEs of formate with different passed charges and (g) the FEs of the H_2 by $Ni(OH)_2$/NF during the MOR||HER at the current density of 20 mA·cm^{-2}. Reproduced with permission from Ref. [98], © Elsevier B.V. 2020. (h) Cryo-electron tomography (cryoET) reconstructed 3D models of $NiMoO_4$·H_2O dissolved in an alkaline solution for 0, 10 and 20 min, respectively. Reproduced with permission from Ref. [100], © Wiley-VCH GmbH 2023.

lower potential (1.39 V vs. RHE), 5-hydroxymethylfurfural could be completely converted to 2,5-furandicarboxylic acid in 90 min with yields and Faraday efficiencies of more than 99% (Figs. 11(e)–11(g)). These studies provide new ideas to improve the catalysts from the perspective of morphology and size.

Zhu et al. revealed the multi-step dissolution of $NiMoO_4$·xH_2O to form ultrathin amorphous $Ni(OH)_2$ nanosheets during electrocatalytic urea oxidation [100]. Firstly, due to the loss of crystallization water, the $NiMoO_4$·xH_2O nanosheets were gradually peeled off from the $NiMoO_4$·xH_2O nanorods in alkaline solution. Subsequently, the remaining crystalline water and molybdenum further dissolve in an alkali solution. Finally, ultrathin amorphous $Ni(OH)_2$ nanosheets are formed (Fig. 11(h)).

$Ni(OH)_2$ nanosheets have been extensively exploited in ECO and previous studies have yielded highly advantageous two-dimensional materials through different synthesis methods. In addition, the thickness of the nanosheets affects the properties of the materials, thus creating novice approaches to minimize the thickness will contribute to the study of this type of materials.

3.2 Design of defects

Defect engineering has been extensively studied due to its

effectiveness in modulating the electronic and geometrical structure of catalysts. Construction of defects is an effective approach to enhance the electrical conductivity, intrinsic activity and active site density of Ni-based catalysts by altering the atomic ordering and reconfiguring the electronic structure to achieve ECO [101].

3.2.1 *Doping of elements*

As a common defect, the introduction of hetero-elements has been extremely widely used in the ECO. Other elements are usually available in the form of doping and loading [102, 103]. The introduction of other elements may be accompanied by vacancies, phase transitions and structural distortions [104, 105]. It can improve the catalytic activity of a catalyst by modulating the electronic structure of the material as well as the interactions between electrons [106–108]. The heteroatoms may shift the Fermi energy levels of the catalysts, thus changing the energy band structure of the catalysts [109, 110]. In addition, it may affect the local charge distribution of the catalyst [111, 112]. The modulation of the charge distribution of the active site promotes the interaction of the active site with the adsorbed material, which improves the catalytic activity [113].

Noble metal catalysts are widely used in electrocatalysis due to their superior catalytic activity [114]. Considering the scarcity and high prices of noble metals, their widespread use is limited. In contrast, metallic nickel is less costly. The outstanding electrical conductivity and adjustable electronic structure contribute to their excellent catalytic activity. And it has excellent durability in alkaline electrolytes [115, 116].

Noble metal single-atom catalysts feature maximum atom utilization and favorable atom dispersion, which can effectively avoid the aggregation of active sites [117–120]. Additionally, the single atom has a unique coordination environment and possesses high catalytic activity [121–124]. The reduction of expensive noble metal loading reduces the cost of the catalysts. Therefore, single-atom catalysts are widely used in electrocatalytic chemicals oxidation [125, 126]. Hu et al. constructed Ni(Co)-Ru-P atomic interfacial sites on Ru single-atom modified NiCoP nanowire arrays (Ru-NiCoP) substrates for electrocatalytic hydrazine oxidation coupled with cathodic hydrogen precipitation (Figs. 12(a)–12(d)) [127]. A two-electrode electrolyzer was employed with Ru-NiCoP as both anode and cathode catalysts with a current density of 522 mA·cm^{-2} at a cell voltage of 0.3 V. The introduction of Ru sites significantly lowered the vacant d-band centers of NiCoP and enhanced the adsorption capacity for $^*N_2H_2$. The reaction energy barrier was lowered, thus increasing the activity of catalyzing hydrazine oxidation. Sun et al. obtained Rh/NiV-LDH for urea oxidation by hydrothermally anchoring Rh single atoms on the NiV-LDH substrate [128]. The dispersed Rh single atoms modify the electronic structure of the parent NiV-LDH substrate. The Rh site also optimizes the adsorption and activation of urea molecules and facilitates the desorption of key intermediates (e.g., CO*/NH*). It greatly reduces the energy barrier of the determining step and thus accelerates UOR activity.

Noble metal-doped nickel-based catalysts are characterized by strong catalytic performance, resource-saving and long lifespan. The design of noble metal-doped nickel-based catalysts has far-

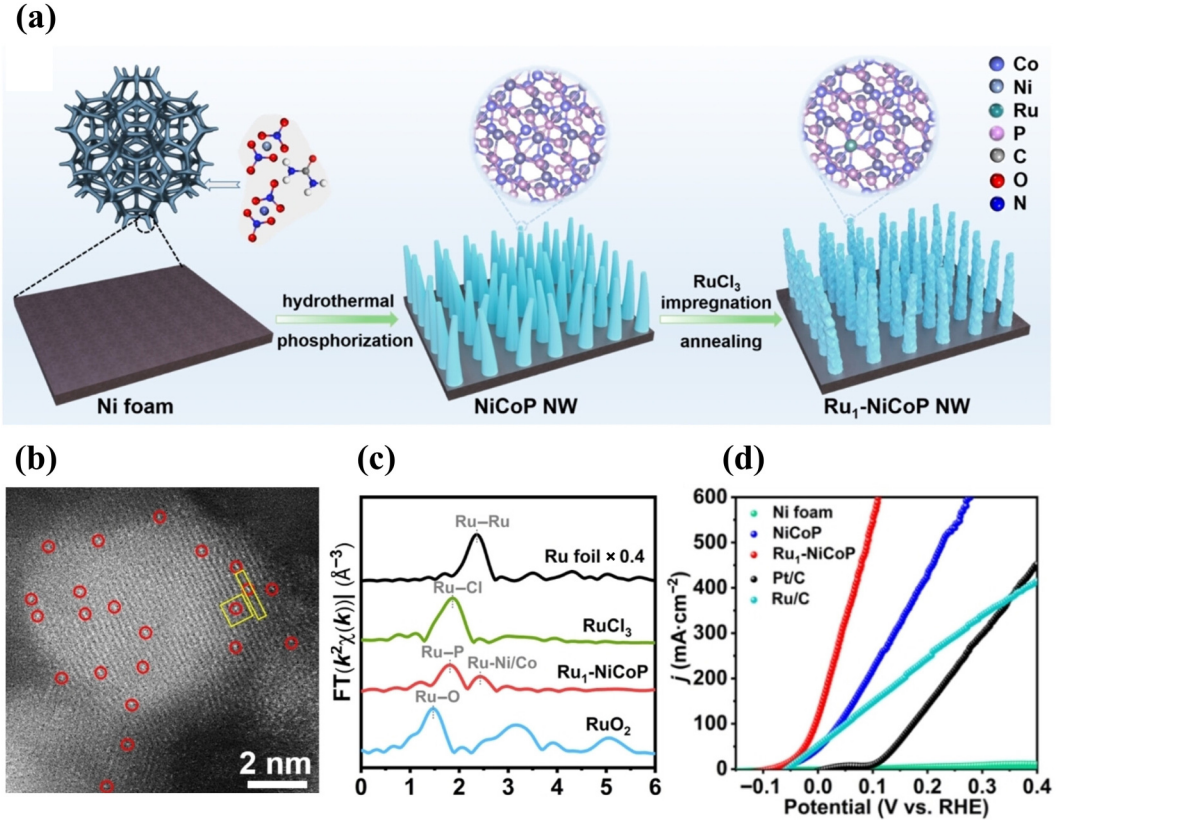

Figure 12 (a) Schematic illustration of the synthesis of Ru_1-NiCoP nanowire arrays. (b) HAADF-STEM image of the Ru_1-NiCoP nanowire arrays. Ru single atoms are highlighted by red circles. (c) The k^2-weighted $\chi(k)$-function of the extended X-ray absorption fine structure (EXAFS) spectra for Ru_1-NiCoP, Ru foil, RuO_2 and $RuCl_3$. (d) HzOR LSV curves of Ru_1-NiCoP nanowire arrays, NiCoP nanowire arrays, bare Ni foam, commercial Pt/C and Ru/C. Reproduced with permission from Ref. [127], © Wiley-VCH GmbH 2023.

reaching significance in the field of electrocatalytic oxidation of chemicals.

Modification of Ni-based catalysts with transition metals has also been extensively studied in the field of electrocatalytic small molecule oxidation. Sun et al. explored the activity of a series of transition metal-doped α-$Ni(OH)_2$ for electrocatalytic benzylamine oxidation [19]. The results showed that Mn doping was the most effective for amine oxidation (Fig. 13(a)). Complete amine conversion with high nitrile selectivity was achieved at 1.40 V vs. RHE. Mn doping promoted the adsorption of amine on NiOOH while maintaining the adsorption capacity of the reactive oxygen-containing intermediates on the adjacent Ni sites. It promotes the anodic efficiency of bimolecular interactions. This work suggests new strategies by comparing amine oxidation with oxygen precipitation.

Ni_3S_2 is widely used in electrocatalysis due to its abundant valence and active centers as well as its superior electrical conductivity [129]. Sun et al. synthesized Co-doped Ni_3S_2 for electrocatalytic 5-hydroxymethylfurfural oxidation by a hydrothermal method using nickel foam as a substrate [130]. X-ray diffraction (XRD) and X-ray photoelectron spectroscopy (XPS) results surfaced that Co was successfully inserted into the Ni_3S_2 lattice, resulting in lattice distortion and reduced crystallinity. Co-doped Ni_3S_2 has an ultra-low onset potential (0.9 V vs. RHE) and at a potential of 1.45 V vs. RHE with high current density (497 $mA{\cdot}cm^{-2}$). Lu et al. tuned the surface electronic structure of β-$Ni(OH)_2$ by co-doping [68]. *In situ* Raman spectroscopy, XPS and high-resolution transmission electron microscopy (HRTEM) revealed the dynamically evolving chemical structure of electron-deficient Ni in β-$Co_{0.1}Ni_{0.9}(OH)_2$ (Fig. 13(b)). Experimental and theoretical calculations indicate that proper Co doping favors the adsorption of OH and HMF.

Wang et al. used $NaBH_4$ to co-reduce Ni^{2+} and Cu^{2+} salt solutions and thereby form NiCu alloy nanoparticles [131]. They were then

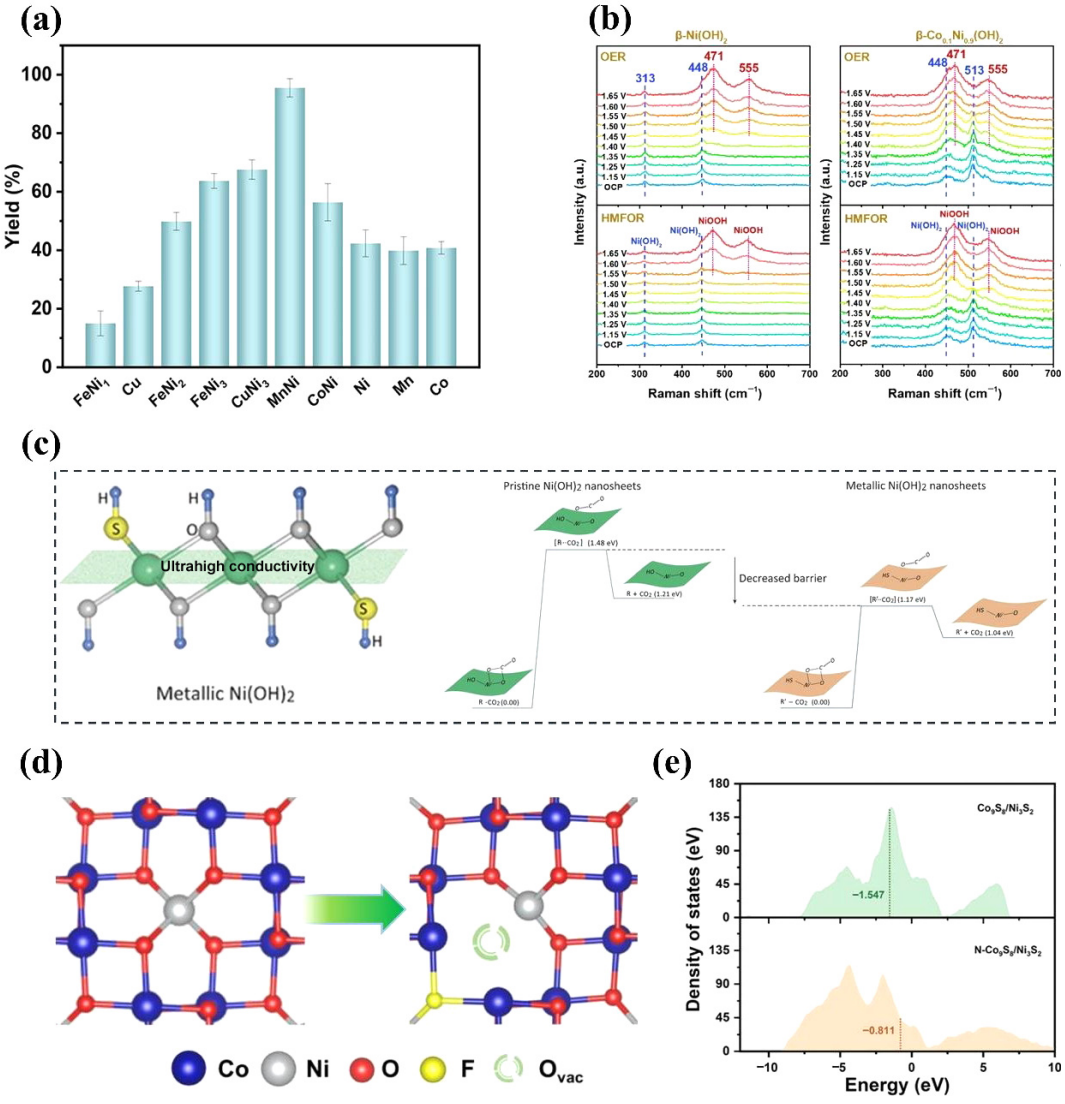

Figure 13 (a) Performance of various catalysts on Ni foam on the benzyl amine (BA) oxidation. Reproduced with permission from Ref. [24], © American Chemical Society 2022. (b) *In situ* Raman spectroscopy of β-$Ni(OH)_2$ and β-$Co_{0.1}Ni_{0.9}(OH)_2$ during the OER and HMF electrooxidation reaction (HMFOR). Reproduced with permission from Ref. [68], © Elsevier Inc. 2023. (c) Kinetics for the CO_2 desorption from electrocatalysts surface. Reproduced with permission from Ref. [137], © WILEY-VCH Verlag GmbH & Co. KGaA, Weinheim 2016. (d) Schematic diagram of the crystal structure for the pristine $NiCo_2O_4$ and F-doped $NiCo_2O_4$. Reproduced with permission from Ref. [139], © Elsevier B.V. 2023. (e) The d band of the DOS of Co_9S_8/Ni_3S_2 and N-Co_9S_8/Ni_3S_2. Reproduced with permission from Ref. [140], © Wiley-VCH GmbH 2023.

electrochemically reconstructed *in situ* using cyclic voltammetry to convert them into Cu-doped NiOOH. The doping of Cu increased the specific surface area of the catalysts and defective sites and facilitated the formation of NiOOH, which has a superior electrocatalytic ethanol oxidation activity. Wang et al. developed a W-doped Ni-based catalyst (Ni-WO_x) for electrocatalytic urea oxidation, which exhibited excellent activity for urea oxidation [132]. The current density was 440 mA·cm^{-2} at 1.6 V vs. RHE. The W-doped catalyst had a high turnover frequency of 0.11 s^{-1}, which was 4.8 times higher than that of the turnover frequency of the non-W-doped catalyst. *In situ* X-ray absorption spectroscopy and X-ray photoelectron spectroscopy indicated that W doping could modulate the local charge distribution of Ni atoms and form NiOOH sites with higher activity, thus accelerating the interfacial catalytic reaction. Qin et al. designed V-doped $Ni(OH)_2$ for electrocatalytic urea oxidation [133]. The doping of V provided more exposed active sites while generating oxygen vacancies. The doping and vacancies synergistically reduced the UOR thermodynamic barrier and significantly enhanced the UOR performance. The above doping of different elements is applied to different applications, which provides ideas for the design of Ni-based catalysts.

Compared with metal doping, nonmetals have excellent compositional and structural flexibility [134]. Their better modification advantages, high natural abundance and relatively low price make them effective doping elements for electrocatalytic performance enhancement [135]. The element sulfur, which is in the same group as oxygen, has a larger atomic radius and is capable of weakening the metal-oxygen bond to create oxygen vacancies and optimize the electronic structure of the catalyst. Lei et al. reported the substitution of sulfur for oxygen in NiFe LDH for surface reconstruction [136]. The doping of S facilitates the modulation of the electronic structure of NiFe LDH and lowers the surface reconstruction energy barrier. Thus, it increases the high valence active sites and improves the catalytic activity. Zhu et al. demonstrated that surface sulfur doping of nickel hydroxide nanosheets effectively avoids the "poisoning" process [137] and gives the material good wettability and effective electron transfer ports (Fig. 13(c)). The introduction of sulfur promoted the urea oxidation reaction (UOR).

Xu et al. constructed NiO/Ni@C heterostructures to increase the number of active sites and thus improve the electrocatalytic activity of NiO [138]. To solve the problem of difficult charge transfer between the heterostructures, this work designed a directed F doping strategy. the introduction of F increased the electron delocalization effect of the catalyst and promoted interfacial electron transfer. Experimental and DFT calculations showed that F doping led to the creation of more oxygen vacancies and became a superior electron conductor, thus promoting the electrocatalytic urea oxidation performance. Yang et al. found that the F-doping strategy enhanced the electrocatalytic 5-hydroxymethylfurfural oxidation by comparing the pristine and F-doped $NiCo_2O_4$ materials [139]. The insertion of F into the O sites weakened the metal-oxygen bonding and spontaneously generated extensive O vacancies (Fig. 13(d)). To preserve the material's electroneutrality, the metal's oxidation state appeared to decrease and the crystal structure seemed to expand. Xie et al. obtained N-doped biphasic metal sulfide catalysts by controlled annealing of biphasic metal sulfides under an ammonia atmosphere [140]. The introduction of N causes some of the metal sulfides in the precursor to be reduced to the corresponding metal phases, which contributes to the improvement of the electron conduction between the material and the adsorbate. In addition, N modulates the d-band center of the material (Fig. 13(e)), which improves the adsorption capacity of the material for urea molecules. The Ni sites of N-Co_9S_8/Ni_3S_2/NF has the lowest urea adsorption energy (−1.91 eV), which is conducive to the occurrence of urea oxidation reaction.

The presence of non-metallic elements helps facilitate substrate oxidation reactions by altering the electronic structure of the precursors, creating numerous oxygen vacancies and improving the adsorption of small molecule substrates on the catalyst surface.

Recently, researchers have designed a series of high-performance catalysts employing multi-element co-doping strategies [141, 142]. The doped elements play different roles in the catalysts and have different functions. In a polymetallic catalytic system, the presence of different metal atoms on the catalyst surface has a synergistic effect and the electronic structure of one metal atom is regulated by another metal atom [143].

Ji et al. prepared a Co, V co-doped NiS_2 electrocatalyst using NiS_2 as a precursor for the electrocatalytic oxidation of urea [144]. In this work, the CO anti-poisoning experiment proved that Co increased the oxidation rate of carbon intermediates produced in the urea oxidation process and effectively inhibited the poisoning of active sites. At the same time, the stability test proves that the stability of the material is improved. In addition, XPS spectra showed that the electron transfer of Ni and Co to V in 3d orbit was carried out, which effectively regulated the electronic structure of the catalyst and improved the catalytic activity (Figs. 14(a) and 14(b)). This work separately demonstrated the effects of different introduced heterogeneous metal elements on the stability and activity of catalysts. Wang et al. reported Co, Ge co-doped nickel-metal hydride oxide catalysts for the first time. Co regulates the NiOOH environment through saturated Co–O bonds [145]. *In situ* Raman test proved that Ge doping reduced the increase of Ni species valence and avoided the competition of oxygen evolution reaction caused by excessive accumulation of NiOOH.

Feng et al. regulated the reactivity by changing the distance between metal atoms on the surface through the strain effect [146]. This work regulates the Ni_2P strain by Cu and Co co-doping strategies near Ni in the periodic table. The lattice strains of mono-doped Cu-Ni_2P/NF, Co-Ni_2P/NF and bimetal co-doped Cu_1Co_2-Ni_2P/NF were further characterized by HRTEM and corresponding fast Fourier transform modes. The tensile strain rate of the Co-Ni_2P/NF lattice is +2.26% and that of the Cu-Ni_2P/NF lattice is +2.71% (Fig. 14(c)). On the contrary, the lattice compression strain rate of Cu_1Co_2-Ni_2P/NF doped with bimetal is −3.62%. The tensile and compressive strain of lattice can decrease and increase the adsorption strength of reaction intermediates respectively [147]. The results of electrochemical tests showed that single Co or Cu doping decreased the hydrazine oxidation activity of Ni_2P while co-doping significantly increased the catalytic activity.

In addition to the co-doping of different metal elements, the co-doping of metal and non-metal elements has also been studied in this field. The co-doping of metallic elements and non-metallic elements can break through the limitation of the traditional single metallic elements and non-metallic elements doping on the promotion of catalytic activity. Yang et al. proved that the co-doping of S and W species $Ni(OH)_2$ made the catalytic reaction kinetics faster, the electrochemically active area larger and promoted the adsorption of the substrate [148]. Element W effectively prevented catalyst poisoning, while element S significantly enhanced charge transfer and urea adsorption capacity.

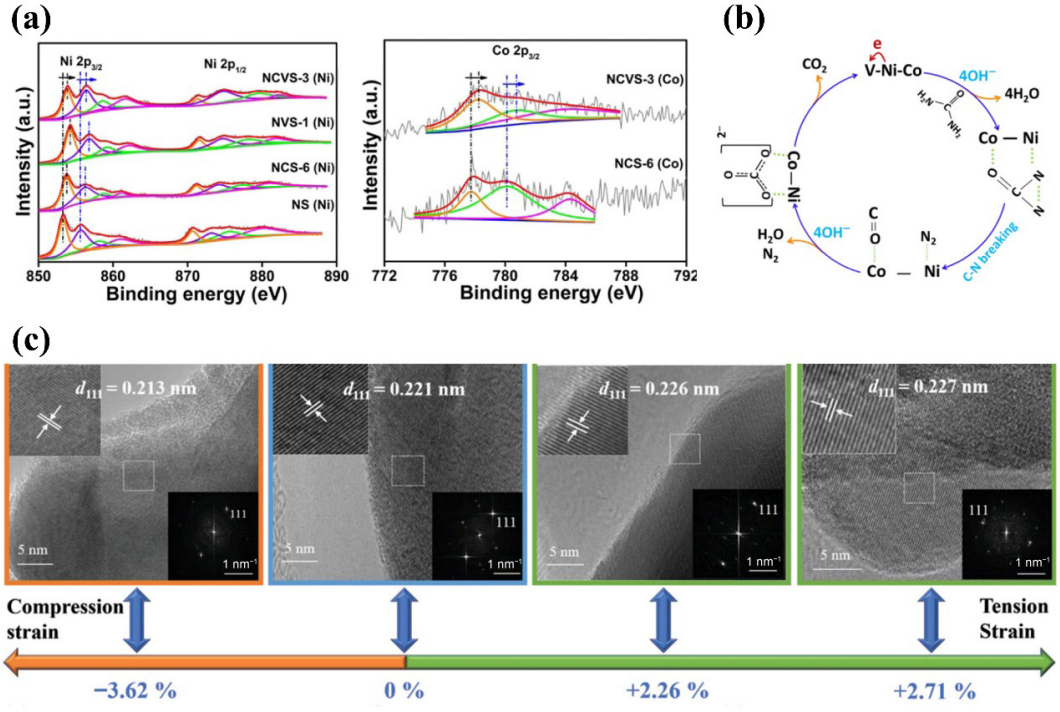

Figure 14 (a) Ni 2p of NS, NCS-6, NVS-1 and NCVS-3; Co $2p_{3/2}$ of NCS-6 and NCVS-3. (b) Possible UOR mechanism on the NCVS-3 electrode. Reproduced with permission from Ref. [144], © American Chemical Society 2021. (c) HRTEM images of Cu_1Co_2-Ni_2P/NF (−3.62%), Ni_2P/NF (0%), Co-Ni_2P/NF (+2.26%) and Cu-Ni_2P/NF (+2.71%). Reproduced with permission from Ref. [146], © Wiley-VCH GmbH 2023.

Kim et al. introduced Co to effectively break the electron neutrality of the catalyst, thereby improving the surface polarity and charge transfer rate of the electrocatalyst, promoting the adsorption of the reactants and improving the catalytic efficiency [149]. The introduction of the more electronegative N element into Ni_2P promotes a higher oxidation state of the metal species, resulting in enhanced electrochemical activity.

Multi-element doping addresses the singular function of a sole element, with multiple elements playing distinct roles in the catalysts to inhibit active sites poisoning or modify the surface polarity of the catalysts, respectively. Notably, multi-element doping may not constitute a straightforward combination of the capabilities, but rather the opposite effects.

3.2.2 *Construction of vacancy defects*

Vacancy defects (point defects) are commonly utilized in electrocatalysis and result from the absence of ions or atoms in the primary material. It can also serve as an additional site for ion insertion, reducing the diffusion barrier for ions [150]. The introduction of vacancy into the catalyst can regulate the electronic structure of the catalyst surface, affect the coordination environment of the active site, optimize the adsorption-free energy of substrate and intermediates on the catalyst surface and facilitate the reaction of substrate on the catalyst surface [151, 152].

Metal oxides or metal hydroxides are common catalysts in the field of ECO. Oxygen vacancy defects have become a common catalyst design strategy and have been extensively studied in ECO. Oxygen vacancy defects can be formed during material synthesis. High-temperature hydrogenation (calcination in H_2, NH_3 and other reducing atmospheres) is a commonly used method to obtain oxygen vacancies [153]. Atmosphere deoxidation is another effective method [154] and the atmosphere is usually vacuum, He, Ar, or N_2. Heterogeneous element doping (metallic element doping or non-metallic element doping) also tends to form oxygen vacancies [155]. There is also extensive research on the formation of oxygen vacancies through surface treatment processes after material synthesis, including plasma and high-energy proton bombardment, laser, stripping and template strategies [156–158]. The temperature control directly affects the formation energy of oxygen vacancy and the concentration of oxygen vacancy increases with the increase of heat treatment temperature. The reducing atmosphere during high-temperature calcination is also conducive to the formation of oxygen vacancies. In addition, the pressure of the gas, the concentration of the reaction solution and doping all have a certain influence on the formation of oxygen vacancy.

Tong et al. controlled the oxygen vacancy on the $NiMoO_4$/NF main material by adjusting the calcination atmosphere [159]. The DFT theoretical calculation shows that the DOS near the Fermi level of the catalyst is obviously enhanced, which indicates the formation of oxygen vacancy. The electrons close to the oxygen vacancy become delocalized, optimizing the adsorption energy of the metal ion center to the urea substrate. Liu et al. prepared oxygen-vacancy-modified NiOOH by ultraviolet (UV) nanosecond laser for electrocatalysis of 5-hydroxymethylfurfural oxidation (Fig. 15(a)) [160]. Synchrotron radiation and original Raman tests showed the formation of oxygen vacancies and the promotion of oxygen vacancies for the formation of NiOOH active centers. After the electrochemical reaction, the conversion rate of the substrate was 97.8% and the FDCA yield of the target product was 96.7%. Although oxygen vacancy has been widely studied because of its low formation energy, its poor stability in an oxygen-rich environment is still a research problem.

The stability of the Ni-based catalyst is reduced mainly due to the formation of NiOOH on the surface and the dissolution of Ni metal. Through the introduction of cation vacancy, the metal dissolution can be effectively alleviated and the lattice distortion can

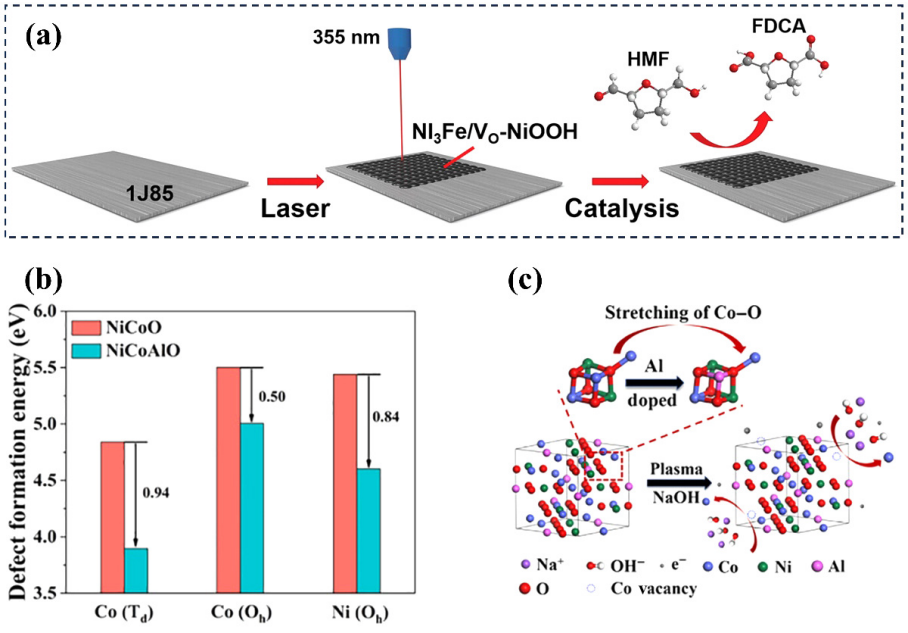

Figure 15 (a) Schematic illustration of the preparation of 1J85-laser electrode by a UV laser. Reproduced with permission from Ref. [160], © Liu, J. B. et al. 2023. (b) The modeling results of NiCoO and NiCoAlO for different cation defect formation energies. (c) Schematic of the Co vacancy generated on the surface of Al-doped $NiCo_2O_4$ under the synergistic effect of plasma and NaOH. Reproduced with permission from Ref. [165], © American Chemical Society 2022.

be reduced [161]. The cation vacancy reduces the surface energy of catalyst and improves the structural stability of catalyst. The metal atoms around the cation vacancy defects are more easily oxidized to form the active center of hydroxyl oxide (NiOOH) than the metal atoms around the anion vacancy defects, so the cation vacancy defects improve the catalytic performance of the main catalyst [162].

Although cationic vacancy has unique electronic and orbital structures, their higher formation makes it more difficult to design and synthesize than oxygen vacancy. Han et al. designed a $LiNiO_2$ layered oxide catalyst for electrocatalytic urea oxidation [163]. Since the adjacent LiO_6 and NiO_6 share edge oxygen atoms, the shared edge oxygen atoms can be activated by introducing Li^+ vacancy into the main catalyst of $LiNiO_2$ to generate non-bonded oxygen states. The unique lattice oxygen oxidation mechanism makes the potential of catalytic urea oxidation lower than that of catalyst autoxidation, resulting in high efficiency and stability of the catalyst up to 160 h. In addition to cation escape caused by specific structures, cation defects generated by optimized synthesis methods have also been extensively studied. Qi et al. modified abundant cation vacancy defects on NiFe LDH nanosheet arrays employing the hydrothermal coordination dissolution method [164]. Compared with ordinary NiFe LDH, the abundant cation vacancy significantly enhances the d-band center of NiFe LDH and effectively regulates the electronic structure of the metal site. NiFe LDH rich in cation defects has excellent electrocatalytic properties for 5-hydroxymethylfurfural oxidation. Doping of heterogeneous elements can not only produce oxygen vacancy but also cation vacancy. Zheng et al. extended the bond length of the Co–O bond by doping the Al atom in $NiCo_2O_4$ to make the crystal lattice expand [165]. Due to the reduction of the bond energy of the Co–O bond, abundant Co defects are preferentially produced under the action of low-temperature plasma (Figs. 15(b) and 15(c)). The production of Co defects results in lower work function, higher carrier concentration and better conductivity of the catalyst. Interface engineering is also an effective method for adjusting electronic structures and producing defects [166]. Lu et al. prepared $NiO\text{-}Co_3O_4$ material with abundant interfacial defects for electrocatalytic oxidation of 5-hydroxymethylfurfural [167]. The characterization proved that the interfacial effect caused abundant Co defects and promoted the formation of NiOOH, thus improving the electrocatalytic performance. These works have important guiding significance for the design of cation vacancy.

3.2.3 *Other defects*

Modulation of edge or helical dislocations results in the formation of line defects in the catalyst. Additionally, regulating grain boundaries and dislocations (planar defects) and introducing cavities and lattice disturbances (bulk defects) can also affect the bonding of active atoms on the surface, thus enhancing the performance of the catalysts. Yang et al. demonstrated that NiCo-LDH-NO_3 synthesized by the ion exchange method is an efficient catalyst for electrocatalytic urea oxidation [168]. Compared with NiCo-LDH and NiCo-LDH-CO_3, NiCo-LDH-NO_3 exhibited better electrocatalytic urea oxidation performance, which was mainly attributed to its more expanded interlayer space. The layered and dislocated structure of the catalyst led to an increase in the electrochemically active area, which promoted the transfer of electrolyte to the surface active center and enhanced the catalytic performance of electrocatalytic urea oxidation. However, there are still some challenges in the research of Ni-based catalysts in the ECO field that need to be studied and solved.

Defects may not exist in a single certain form and doping or vacancy defects can further lead to lattice disorder. Therefore, designing catalysts from a defect perspective is abundant and effective.

3.3 Construction of heterojunction

Due to the limited performance of single-component catalysts, the construction of heterojunction has been widely used in the design of catalysts [169]. The stability, conductivity and hydrophilicity of

the material can be effectively adjusted through the reasonable combination of components with different properties [170–172]. The difference in Fermi level between different components of heterojunction results in the transfer of interfacial charge, which effectively regulates the interfacial charge distribution [173, 174]. Electron transfer is facilitated by bonding at different phase interfaces. In addition, different components may cause lattice strain to occur, thus changing the adsorption energy of the intermediate [175].

Qi et al. designed nickel boride/nickel heterojunction catalysts for electrocatalytic oxidation (Fig. 16(a)) [176]. The electron transfer at the interface is analyzed by differential charge density diagram and Bard charge. DFT theoretical calculation shows that the formation of CH_2O is more likely to occur on nickel boride/nickel heterostructures than on nickel boride and nickel. Moreover, the adsorption energy barrier of $*CH_2O$ intermediate on the heterostructure is lower than that on Ni_3B and Ni, which effectively promotes the reaction (Fig. 16(b)). Xie et al. prepared a Ni_3N/Co_3N heterojunction catalyst for electrocatalytic oxidation of hydrazine hydrate [177]. Through XPS analysis, it is found that the constructed heterojunction structure can effectively regulate the electronic structure of the material. The effective interfacial coupling significantly reduces the reaction energy barrier during the oxidative dehydrogenation of hydrazine hydrate and thus enhances the oxidative activity of hydrazine hydrate under alkaline conditions (Fig. 16(c)). Luo et al. reported the final application of $Ni(OH)_2$/NiFeP heterojunction catalyst in electrocatalysis of 5-hydroxymethylfurfural oxidation [178]. Physical characterization proved that in KOH alkaline solution, NiFeP catalyst formed $Ni(OH)_2$/NiFeP heterostructures *in situ* with the increase of potential and further oxidation occurred to NiOOH/NiFeP. The spontaneous chemical reaction between 5-hydroxymethylfurfural and NiOOH blocks the oxidation of NiOOH to a higher valence state, which effectively inhibits the occurrence of the side reaction oxygen evolution. The complexity of synergistic effects and electron interactions in heterostructure requires advanced characterization techniques for further exploration.

Therefore, the discrepancy in Fermi energy levels between components contributes to the transfer of interfacial charges, which modulates the interfacial charge distribution. Bonding at the interfaces of different phases promotes the transfer of electrons. The synergistic effects and electronic interaction relationships in heterojunctions are complex and still require the exploration of advanced characterization techniques to investigate.

4 Conclusions and outlook

In this review, recent advances in the application of Ni-based catalysts for ECO are presented. The inexpensive Ni-based catalysts have relatively superior catalytic properties and their oxides or hydroxides are highly resistant to corrosion under alkaline conditions. These properties have allowed Ni-based catalysts to be

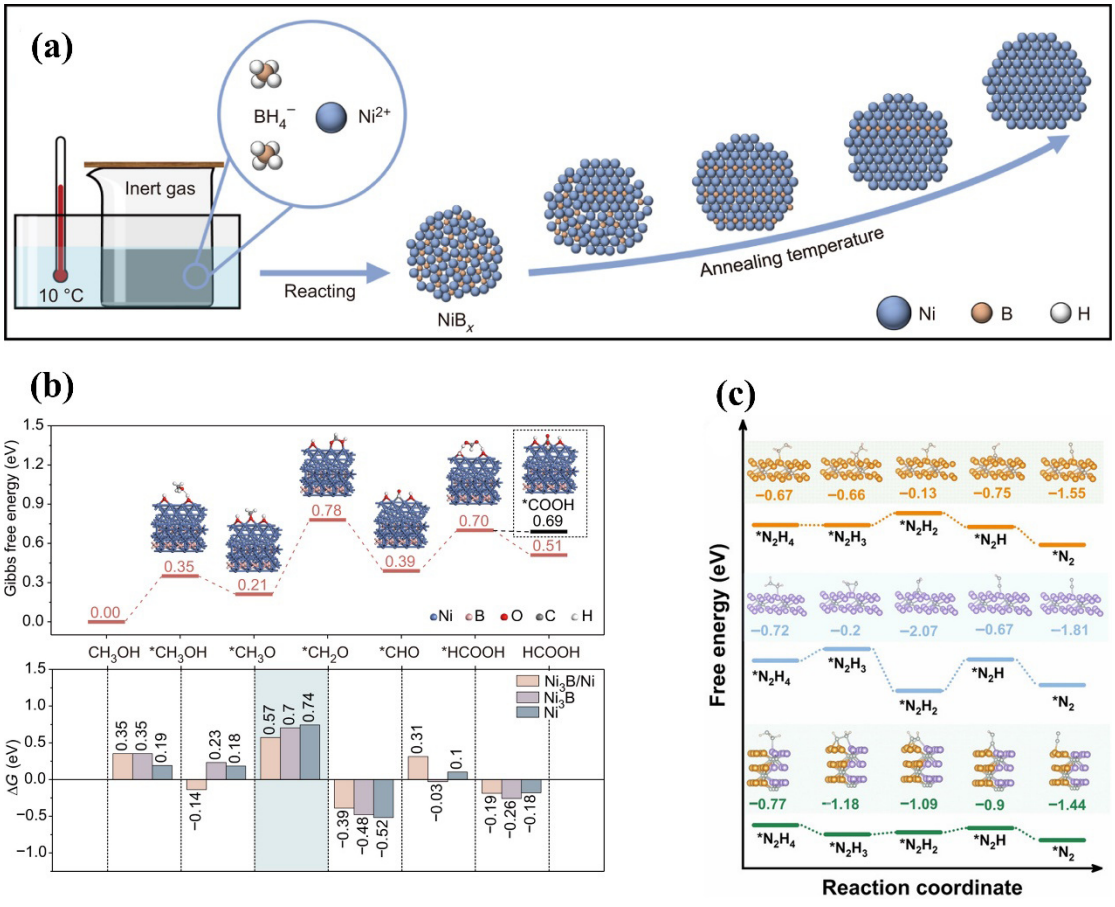

Figure 16 (a) Schematic diagram of the Ni_3B/Ni preparation. (b) Gibbs free energy diagram of MOR occurring on Ni_3B (001)/Ni (111) heterostructure (upper) and the change in Gibbs free energy between the steps on different surfaces (lower). Reproduced with permission from Ref. [176], © Qi, Y. B. et al. 2022. (c) The most stable configurations of each adsorbed intermediate and the free-energy profiles for HzOR on the Ni_3N, Co_3N and Ni_3N–Co_3N heterostructure surfaces. Reproduced with permission from Ref. [177], © Wiley-VCH GmbH 2020.

widely used in ECO. In addition, modification strategies of Ni-based catalysts to achieve the promotion of Ni-based catalysts towards NiOOH reconfiguration, exposure of NiOOH active sites and enhancement of the intrinsic activity of the catalysts are highlighted. The specific surface area and intrinsic activity of the catalysts can be increased by modulating the size and morphology of the catalysts, thus improving the catalytic performance of the catalysts. The doping strategy is possibly accompanied by vacancies, phase transitions and structural distortions. It can modulate the electronic structure of the material as well as the interactions between electrons. Heteroatoms may shift the Fermi energy levels of the catalyst, thus changing the energy band structure of the catalyst. Furthermore, it potentially affects the local charge distribution of the catalyst. The introduction of anionic defects or cationic defects can modulate the electronic structure of the catalyst surface and affect the coordination environment of the active site. Its optimization of the free energy of adsorption of substrates and intermediates on the catalyst surface promotes the reaction of substrates on the catalyst surface. The rational combination of different components by constructing heterojunctions can effectively regulate the stability, conductivity and hydrophilicity of the materials.

However, there are still some challenges in the research of Ni-based catalysts in the ECO field that need to be studied and solved.

(1) NiOOH acts as an oxidant on the oxidizing substrate and is reduced back to $Ni(OH)_2$ by the substrate. Meanwhile, $Ni(OH)_2$ is continuously oxidized to NiOOH at positive potential. However, the formation potential of NiOOH in this mechanism is a difficult limiting condition to break through. The formation potential of NiOOH inhibits the reduction of NiOOH and thus the oxidation of the substrate. Therefore, it is necessary to seek new methods and discuss new mechanisms to break through the potential limitation.

(2) According to previous studies, NiOOH promotes both ECO and OER. The substrate is electrically neutral, while OH^- is negatively charged. When the potential exceeds 1.48 V vs. RHE, the substrate's adsorption on NiOOH species is significantly weaker compared to the adsorption of OH^- on NiOOH. As a result, the sites of NiOOH for the substrate reaction are occupied by OH^-, thereby inhibiting the oxidation of the substrate. The competition between OER and ECO will inevitably diminish the utilization rate of charge. Therefore, it is a necessity to attempt to achieve industrial current densities with superior stability at potentials lower than 1.48 V vs. RHE. This will require seeking new modification strategies for finer control of the catalyst.

(3) Although efficient oxidation of substrates has been achieved by modulating the surface electronic and geometrical structure of Ni-based materials, the specific relationship between morphology, defects and selectivity remains unclear. In addition, the effects of different modulation strategies on the substrate reaction paths are not explicit. Therefore, modern *in situ* spectroscopic tools combined with DFT theoretical calculations should be utilized to trace the structural evolution and the actual reaction mechanism during the reaction process, which will provide theoretical guidance for the design and development of high-efficiency catalysts.

In conclusion, Ni-based materials offer unique advantages and wide-ranging application potential in ECO. As we enhance our understanding of the relationship between the structure and properties of Ni-based catalysts, improve characterization tools and gain insight into the catalytic process mechanism, we can intentionally design and synthesize new Ni-based catalysts to further advance ECO catalysis. We expect this review to be helpful for researchers interested in this field.

Data availability

Not applicable.

Acknowledgements

This work was supported by the National Natural Science Foundation of China (Nos. 52072152 and 51802126), the Jiangsu University Jinshan Professor Fund, the Jiangsu Specially-Appointed Professor Fund, Open Fund from Guangxi Key Laboratory of Electrochemical Energy Materials, Zhenjiang "Jinshan Talents" Project 2021, China PostDoctoral Science Foundation (No. 2022M721372), "Doctor of Entrepreneurship and Innovation" in Jiangsu Province (No. JSSCBS20221197), the Postgraduate Research & Practice Innovation Program of Jiangsu Province (Nos. KYCX22_3645 and KYCX24_3964) and Student Research Project of Jiangsu University (No. 23A586).

Declaration of competing interest

All the contributing authors report no conflict of interests in this work.

Author contribution statement

J. W. Y.: Data curation, project administration, validation, writing manuscript. Y. L. L.: Data curation, project administration, validation. N. Y. L.: Project administration, funding acquisition. Y. X. L.: Writing manuscript, data curation. Y. Y. C.: Validation, data curation. P. C.: Data curation, writing manuscript. Y. X. L.: Project administration, writing manuscript. X. Y. Y.: Writing manuscript. X. Y. Z.: Data curation. H. T. L.: Project administration, funding acquisition, writing manuscript. All the authors have approved the final manuscript.

Use of AI statement

None.

References

[1] Liu, Y. H.; Zhang, K. W.; Zhang, D. X.; Dong, W. X.; Jiang, T. Y.; Zhou, H. B.; Li, L. X.; Mao, B. D. Industrial stainless steel meshes for efficient electrocatalytic hydrogen evolution. *J. Energy Storage* **2021**, *41*, 102844.

[2] Zhang, M. Y.; Zhou, W. D.; Yan, X. H.; Huang, X. P.; Wu, S. T.; Pan, J. M.; Shahnavaz, Z.; Li, T.; Yu, X. Y. Sodium dodecyl sulfate intercalated two-dimensional nickel-cobalt layered double hydroxides to synthesize multifunctional nanomaterials for supercapacitors and electrocatalytic hydrogen evolution. *Fuel* **2023**, *333*, 126323.

[3] Guan, S. Y.; Yuan, Z. L.; Zhao, S. Q.; Zhuang, Z. C.; Zhang, H. H.; Shen, R. F.; Fan, Y. P.; Li, B. J.; Wang, D. S.; Liu, B. Z. Efficient hydrogen generation from ammonia borane hydrolysis on a tandem ruthenium-platinum-titanium catalyst. *Angew. Chem., Int. Ed.* **2024**, *63*, e202408193.

[4] Zhu, P.; Xiong, X.; Wang, D. S. Regulations of active moiety in single atom catalysts for electrochemical hydrogen evolution reaction. *Nano Res.* **2022**, *15*, 5792–5815.

[5] Li, Z. H.; Yan, Y. F.; Xu, S. M.; Zhou, H.; Xu, M.; Ma, L. N.; Shao,

M. F.; Kong, X. G.; Wang, B.; Zheng, L. R. et al. Alcohols electrooxidation coupled with H_2 production at high current densities promoted by a cooperative catalyst. *Nat. Commun.* **2022**, *13*, 147.

[6] Bhuvanendran, N.; Ravichandran, S.; Jayaseelan, S. S.; Xu, Q.; Khotseng, L.; Su, H. N. Improved bi-functional oxygen electrocatalytic performance of Pt-Ir alloy nanoparticles embedded on MWCNT with Pt-enriched surfaces. *Energy* **2020**, *211*, 118695.

[7] Dong, W. X.; Zhou, H. B.; Mao, B. D.; Zhang, Z. Y.; Liu, Y. S.; Liu, Y. H.; Li, F. H.; Zhang, D. Q.; Zhang, D. X.; Shi, W. D. Efficient MOF- derived V–Ni_3S_2 nanosheet arrays for electrocatalytic overall water splitting in alkali. *Int. J. Hydrogen Energy* **2021**, *46*, 10773–10782.

[8] Zhu, J. J.; Lu, Y. K.; Liu, C. C.; Cheng, T.; Xu, S. J.; Li, D.; Jiang, D. L. Template confined construction of Fe-NiCoP/NiCoP/NF heterostructures for highly efficient electrocatalytic oxygen evolution reaction. *Int. J. Hydrogen Energy* **2021**, *46*, 37746–37756.

[9] Chen, F. J.; Mu, X. Q.; Zhou, J. L.; Wang, S. C.; Liu, Z. Y.; Zhou, D. Y.; Liu, S. L.; Wang, D. S.; Dai, Z. H. Engineering the active sites of MOF-derived catalysts: From oxygen activation to activate metal-air batteries. *Chin. J. Chem.* **2024**, in press, DOI: 10.1002/cjoc.202400332.

[10] Xiao, L.; Dai, W. D.; Mou, S. Y.; Wang, X. Y.; Cheng, Q.; Dong, F. Coupling electrocatalytic cathodic nitrate reduction with anodic formaldehyde oxidation at ultra-low potential over Cu_2O. *Energy Environ. Sci.* **2023**, *16*, 2696–2704.

[11] Wang, Q. X.; Liu, J. F.; Li, T.; Zhang, T.; Arbiol, J.; Yan, S. X.; Wang, Y.; Li, H. M.; Cabot, A. Pd_2Ga nanorods as highly active bifunctional catalysts for electrosynthesis of acetic acid coupled with hydrogen production. *Chem. Eng. J.* **2022**, *446*, 136878.

[12] Wang, Y.; Zheng, X. B.; Wang, D. S. Design concept for electrocatalysts. *Nano Res.* **2022**, *15*, 1730–1752.

[13] Li, R. Z.; Wang, D. S. Understanding the structure–performance relationship of active sites at atomic scale. *Nano Res.* **2022**, *15*, 6888–6923.

[14] Zhang, Z. Y.; Xin, L.; Qi, J.; Chadderdon, D. J.; Sun, K.; Warsko, K. M.; Li, W. Z. Selective electro-oxidation of glycerol to tartronate or mesoxalate on Au nanoparticle catalyst via electrode potential tuning in anion-exchange membrane electro-catalytic flow reactor. *Appl. Catal. B: Environ.* **2014**, *147*, 871–878.

[15] Jiao, S. L.; Fu, X. W.; Wang, S. Y.; Zhao, Y. Perfecting electrocatalysts via imperfections: Towards the large-scale deployment of water electrolysis technology. *Energy Environ. Sci.* **2021**, *14*, 1722–1770.

[16] Thiyagarajan, D.; Gao, M. Y.; Sun, L.; Dong, X. C.; Zheng, D. H.; Wahab, M. A.; Will, G.; Lin, J. J. Nanoarchitectured porous Cu-CoP nanoplates as electrocatalysts for efficient oxygen evolution reaction. *Chem. Eng. J.* **2022**, *432*, 134303.

[17] Taitt, B. J.; Nam, D. H.; Choi, K. S. A comparative study of nickel, cobalt, and iron oxyhydroxide anodes for the electrochemical oxidation of 5-hydroxymethylfurfural to 2,5-furandicarboxylic acid. *ACS Catal.* **2019**, *9*, 660–670.

[18] Zheng, X. B.; Li, B. B.; Wang, Q. S.; Wang, D. S.; Li, Y. D. Emerging low-nuclearity supported metal catalysts with atomic level precision for efficient heterogeneous catalysis. *Nano Res.* **2022**, *15*, 7806–7839.

[19] Hassaninejad-Darzi, S. K. Encapsulation of a nickel Salen complex in nanozeolite LTA as a carbon paste electrode modifier for electrocatalytic oxidation of hydrazine. *Chin. J. Catal.* **2018**, *39*, 283–296.

[20] Li, D.; Zhou, X. M.; Ruan, Q. D.; Liu, L. L.; Liu, J. Y.; Wang, B.; Wang, Y. C.; Zhang, X. L.; Chen, R. S.; Ni, H. W. et al. Suppression of passivation on nickel hydroxide in electrocatalytic urea oxidization. *Adv. Funct. Mater.* **2024**, *34*, 2313680.

[21] Liu, C. F.; Shi, X. R.; Yue, K. H.; Wang, P. J.; Zhan, K.; Wang, X. Y.; Xia, B. Y.; Yan, Y. S-species-evoked high-valence $Ni^{2+\delta}$ of the evolved β-$Ni(OH)_2$ electrode for selective oxidation of 5-hydroxymethylfurfural. *Adv. Mater.* **2023**, *35*, 2211177.

[22] Dubale, A. A.; Zheng, Y. Y.; Wang, H. L.; Hübner, R.; Li, Y.; Yang, J.; Zhang, J. W.; Sethi, N. K.; He, L. Q.; Zheng, Z. K. et al. High-performance bismuth-doped nickel aerogel electrocatalyst for the methanol oxidation reaction. *Angew. Chem., Int. Ed.* **2020**, *59*, 13891–13899.

[23] Xu, Y.; Liu, M. Y.; Wang, S. Q.; Ren, K. L.; Wang, M. Z.; Wang, Z. Q.; Li, X. N.; Wang, L.; Wang, H. J. Integrating electrocatalytic hydrogen generation with selective oxidation of glycerol to formate over bifunctional nitrogen-doped carbon coated nickel-molybdenum-nitrogen nanowire arrays. *Appl. Catal. B: Environ.* **2021**, *298*, 120493.

[24] Sun, Y. X.; Shin, H.; Wang, F. Y.; Tian, B. L.; Chiang, C. W.; Liu, S. T.; Li, X. S.; Wang, Y. Q.; Tang, L. Y.; Goddard III, W. A. et al. Highly selective electrocatalytic oxidation of amines to nitriles assisted by water oxidation on metal-doped α-$Ni(OH)_2$. *J. Am. Chem. Soc.* **2022**, *144*, 15185–15192.

[25] Cui, X.; Chen, M. L.; Xiong, R.; Sun, J.; Liu, X. W.; Geng, B. Y. Ultrastable and efficient H_2 production via membrane-free hybrid water electrolysis over a bifunctional catalyst of hierarchical Mo-Ni alloy nanoparticles. *J. Mater. Chem. A* **2019**, *7*, 16501–16507.

[26] Khakyzadeh, V.; Sediqi, S. The electro-oxidation of primary alcohols via a coral-shaped cobalt metal-organic framework modified graphite electrode in neutral media. *Sci. Rep.* **2022**, *12*, 8560.

[27] Peng, K.; Bhuvanendran, N.; Ravichandran, S.; Zhang, W. Q.; Ma, Q.; Xing, L.; Xu, Q.; Khotseng, L.; Su, H. N. Carbon supported PtPdCr ternary alloy nanoparticles with enhanced electrocatalytic activity and durability for methanol oxidation reaction. *Int. J. Hydrogen Energy* **2020**, *45*, 22752–22760.

[28] Badalyan, A.; Stahl, S. S. Cooperative electrocatalytic alcohol oxidation with electron-proton-transfer mediators. *Nature* **2016**, *535*, 406–410.

[29] Bender, M. T.; Warburton, R. E.; Hammes-Schiffer, S.; Choi, K. S. Understanding hydrogen atom and hydride transfer processes during electrochemical alcohol and aldehyde oxidation. *ACS Catal.* **2021**, *11*, 15110–15124.

[30] Fleischmann, M.; Korinek, K.; Pletcher, D. The oxidation of organic compounds at a nickel anode in alkaline solution. *J. Electroanal. Chem. Interfacial Electrochem.* **1971**, *31*, 39–49.

[31] Bender, M. T.; Choi, K. S. Electrochemical dehydrogenation pathways of amines to nitriles on NiOOH. *JACS Au* **2022**, *2*, 1169–1180.

[32] McLoughlin, E. A.; Armstrong, K. C.; Waymouth, R. M. Electrochemically regenerable hydrogen atom acceptors: Mediators in electrocatalytic alcohol oxidation reactions. *ACS Catal.* **2020**, *10*, 11654–11662.

[33] Bender, M. T.; Lam, Y. C.; Hammes-Schiffer, S.; Choi, K. S. Unraveling two pathways for electrochemical alcohol and aldehyde oxidation on NiOOH. *J. Am. Chem. Soc.* **2020**, *142*, 21538–21547.

[34] Hao, Y. M.; Li, J. L.; Cao, X. T.; Meng, L. S.; Wu, J. X.; Yang, X. J.; Li, Y. F.; Liu, Z. P.; Gong, M. Origin of the universal potential-dependent organic oxidation on nickel oxyhydroxide. *ACS Catal.* **2023**, *13*, 2916–2927.

[35] Zhu, B. T.; Dong, B.; Wang, F.; Yang, Q. F.; He, Y. P.; Zhang, C. J.; Jin, P.; Feng, L. Unraveling a bifunctional mechanism for methanol-to-formate electro-oxidation on nickel-based hydroxides. *Nat. Commun.* **2023**, *14*, 1686.

[36] Huang, H. L.; Yu, C.; Han, X. T.; Huang, H. W.; Wei, Q. B.; Guo, W.; Wang, Z.; Qiu, J. S. Ni, Co hydroxide triggers electrocatalytic production of high-purity benzoic acid over 400 $mA \cdot cm^{-2}$. *Energy Environ. Sci.* **2020**, *13*, 4990–4999.

[37] Goetz, M. K.; Bender, M. T.; Choi, K. S. Predictive control of selective secondary alcohol oxidation of glycerol on NiOOH. *Nat. Commun.* **2022**, *13*, 5848.

[38] Luo, H.; Barrio, J.; Sunny, N.; Li, A.; Steier, L.; Shah, N.; Stephens,

I. E. L.; Titirici, M. M. Progress and perspectives in photo- and electrochemical-oxidation of biomass for sustainable chemicals and hydrogen production. *Adv. Energy Mater.* **2021**, *11*, 2101180.

[39] Luo, H.; Yukuhiro, V. Y.; Fernández, P. S.; Feng, J. Y.; Thompson, P.; Rao, R. R.; Cai, R. S.; Favero, S.; Haigh, S. J.; Durrant, J. R. et al. Role of Ni in PtNi bimetallic electrocatalysts for hydrogen and value-added chemicals coproduction via glycerol electrooxidation. *ACS Catal.* **2022**, *12*, 14492–14506.

[40] Li, S. L.; Ma, P. J.; Gao, C. L.; Liu, L. J.; Wang, X. L.; Shakour, M.; Chernikov, R.; Wang, K. W.; Liu, D. M.; Ma, R. G. et al. Reconstruction-induced NiCu-based catalysts towards paired electrochemical refining. *Energy Environ. Sci.* **2022**, *15*, 3004–3014.

[41] Si, D.; Xiong, B. Y.; Chen, L. S.; Shi, J. L. Highly selective and efficient electrocatalytic synthesis of glycolic acid in coupling with hydrogen evolution. *Chem. Catal.* **2021**, *1*, 941–955.

[42] Yan, Y. F.; Zhou, H.; Xu, S. M.; Yang, J. R.; Hao, P. J.; Cai, X.; Ren, Y.; Xu, M.; Kong, X. G.; Shao, M. F. et al. Electrocatalytic upcycling of biomass and plastic wastes to biodegradable polymer monomers and hydrogen fuel at high current densities. *J. Am. Chem. Soc.* **2023**, *145*, 6144–6155.

[43] Liu, F. L.; Gao, X. T.; Shi, R.; Guo, Z. X.; Tse, E. C. M.; Chen, Y. Concerted and selective electrooxidation of polyethylene-terephthalate-derived alcohol to glycolic acid at an industry-level current density over a Pd-Ni$(OH)_2$ catalyst. *Angew. Chem., Int. Ed.* **2023**, *62*, e202300094.

[44] Chen, W.; Xu, L. T.; Zhu, X. R.; Huang, Y. C.; Zhou, W.; Wang, D. D.; Zhou, Y. Y.; Du, S. Q.; Li, Q. L.; Xie, C. et al. Unveiling the electrooxidation of urea: Intramolecular coupling of the N–N bond. *Angew. Chem., Int. Ed.* **2021**, *60*, 7297–7307.

[45] Li, J. N.; Li, J. L.; Liu, T.; Chen, L.; Li, Y. F.; Wang, H. L.; Chen, X. R.; Gong, M.; Liu, Z. P.; Yang, X. J. Deciphering and suppressing over-oxidized nitrogen in nickel-catalyzed urea electrolysis. *Angew. Chem., Int. Ed.* **2021**, *60*, 26656–26662.

[46] Song, Y. C.; Woo, J. H.; Oh, G. G.; Kim, D. H.; Lee, C. Y.; Kim, H. W. External electric field promotes ammonia stripping from wastewater. *Water Res.* **2021**, *203*, 117518.

[47] Vikrant, K.; Kim, K. H.; Dong, F.; Giannakoudakis, D. A. Photocatalytic platforms for removal of ammonia from gaseous and aqueous matrixes: Status and challenges. *ACS Catal.* **2020**, *10*, 8683–8716.

[48] Lyu, Z. H.; Fu, J. J.; Tang, T.; Zhang, J. N.; Hu, J. S. Design of ammonia oxidation electrocatalysts for efficient direct ammonia fuel cells. *EnergyChem* **2023**, *5*, 100093.

[49] Wu, L.; Tang, D. J.; Xue, J.; Liu, S. Q.; Wang, J. M.; Ji, H. W.; Chen, C. C.; Zhang, Y. C.; Zhao, J. C. Competitive non-radical nucleophilic attack pathways for NH_3 oxidation and H_2O oxidation on hematite photoanodes. *Angew. Chem., Int. Ed.* **2022**, *61*, e202214580.

[50] Oswin, H. G.; Salomon, M. The anodic oxidation of ammonia at platinum black electrodes in aqueous KOH electrolyte. *Can. J. Chem.* **1963**, *41*, 1686–1694.

[51] Siddharth, K.; Chan, Y.; Wang, L.; Shao, M. H. Ammonia electro-oxidation reaction: Recent development in mechanistic understanding and electrocatalyst design. *Curr. Opin. Electrochem.* **2018**, *9*, 151–157.

[52] Gerischer, H.; Mauerer, A. Untersuchungen zur anodischen oxidation von Ammoniak an Platin-Elektroden. *J. Electroanal. Chem. Interfacial Electrochem.* **1970**, *25*, 421–433.

[53] Tian, Y. R.; Mao, Z. X.; Wang, L. Q.; Liang, J. Green chemistry: Advanced electrocatalysts and system design for ammonia oxidation. *Small Struct.* **2023**, *4*, 2200266.

[54] Almomani, F.; Bhosale, R.; Khraisheh, M.; Kumar, A.; Tawalbeh, M. Electrochemical oxidation of ammonia on nickel oxide nanoparticles. *Int. J. Hydrogen Energy* **2020**, *45*, 10398–10408.

[55] Allagui, A.; Sarfraz, S.; Ntais, S.; Al momani, F.; Baranova, E. A. Electrochemical behavior of ammonia on $Ni_{98}Pd_2$ nano-structured catalyst. *Int. J. Hydrogen Energy* **2014**, *39*, 41–48.

[56] Li, Y. P.; Niu, S. W.; Liu, P. G.; Pan, R. R.; Zhang, H. K.; Ahmad, N.; Shi, Y.; Liang, X.; Cheng, M. Y.; Chen, S. H. et al. Ruthenium nanoclusters and single atoms on α-MoC/N-doped carbon achieves low-input/input-free hydrogen evolution via decoupled/coupled hydrazine oxidation. *Angew. Chem., Int. Ed.* **2024**, *63*, e202316755.

[57] Liu, Q.; Liao, X. B.; Tang, Y. H.; Wang, J. H.; Lv, X. Z.; Pan, X. L.; Lu, R. H.; Zhao, Y.; Yu, X. Y.; Wu, H. B. Low-coordinated cobalt arrays for efficient hydrazine electrooxidation. *Energy Environ. Sci.* **2022**, *15*, 3246–3256.

[58] Zhou, L.; Shao, M. F.; Zhang, C.; Zhao, J. W.; He, S.; Rao, D. M.; Wei, M.; Evans, D. G.; Duan, X. Hierarchical CoNi-sulfide nanosheet arrays derived from layered double hydroxides toward efficient hydrazine electrooxidation. *Adv. Mater.* **2017**, *29*, 1604080.

[59] Wen, H.; Gan, L. Y.; Dai, H. B.; Wen, X. P.; Wu, L. S.; Wu, H.; Wang, P. *In situ* grown Ni phosphide nanowire array on Ni foam as a high-performance catalyst for hydrazine electrooxidation. *Appl. Catal. B: Environ.* **2019**, *241*, 292–298.

[60] Zhang, J. H.; Liu, Y.; Li, J. M.; Jin, X.; Li, Y. P.; Qian, Q. Z.; Wang, Y. X.; El-Harairy, A.; Li, Z. Y.; Zhu, Y. et al. Vanadium substitution steering reaction kinetics acceleration for Ni_3N nanosheets endows exceptionally energy-saving hydrogen evolution coupled with hydrazine oxidation. *ACS Appl. Mater. Interfaces* **2021**, *13*, 3881–3890.

[61] Xu, X. F.; Chen, H. C.; Li, L. F.; Humayun, M.; Zhang, X.; Sun, H. C.; Debecker, D. P.; Zhang, W. J.; Dai, L. M.; Wang, C. D. Leveraging metal nodes in metal-organic frameworks for advanced anodic hydrazine oxidation assisted seawater splitting. *ACS Nano* **2023**, *17*, 10906–10917.

[62] Wang, Y.; Xue, Y. Y.; Yan, L. T.; Li, H. P.; Li, Y. P.; Yuan, E. H.; Li, M.; Li, S. N.; Zhai, Q. G. Multimetal incorporation into 2D conductive metal-organic framework nanowires enabling excellent electrocatalytic oxidation of benzylamine to benzonitrile. *ACS Appl. Mater. Interfaces* **2020**, *12*, 24786–24795.

[63] Wei, K. L.; Wang, X.; Jiao, X. L.; Li, C.; Chen, D. R. Self-supported 2D Fe-doped Ni-MOF nanosheets as highly efficient and stable electrocatalysts for benzylamine oxidation. *Appl. Surf. Sci.* **2022**, *578*, 152065.

[64] Ding, Y.; Miao, B. Q.; Li, S. N.; Jiang, Y. C.; Liu, Y. Y.; Yao, H. C.; Chen, Y. Benzylamine oxidation boosted electrochemical water-splitting: Hydrogen and benzonitrile co-production at ultra-thin Ni_2P nanomeshes grown on nickel foam. *Appl. Catal. B: Environ.* **2020**, *268*, 118393.

[65] Ren, Z.; Yang, Y. S.; Wang, S.; Li, X. L.; Feng, H. S.; Wang, L.; Li, Y. M.; Zhang, X.; Wei, M. Pt atomic clusters catalysts with local charge transfer towards selective oxidation of furfural. *Appl. Catal. B: Environ.* **2021**, *295*, 120290.

[66] Liu, B. Y.; Zhang, M.; Liu, Y. Y.; Wang, Y. C.; Yan, K. Electrodeposited 3D hierarchical NiFe microflowers assembled from nanosheets robust for the selective electrooxidation of furfuryl alcohol. *Green Energy Environ.* **2023**, *8*, 874–882.

[67] Fang, Z. Y.; Zhang, P. L.; Wang, M.; Li, F. S.; Wu, X. J.; Fan, K.; Sun, L. C. Selective electro-oxidation of alcohols to the corresponding aldehydes in aqueous solution via Cu(III) intermediates from CuO nanorods. *ACS Sustainable Chem. Eng.* **2021**, *9*, 11855–11861.

[68] Lu, L. Y.; Wen, C. Y.; Wang, H. Y.; Li, Y. H.; Wu, J. C.; Wang, C. G. Tailoring the electron structure and substrate adsorption energy of Ni hydroxide via Co doping to enhance the electrooxidation of biomass-derived chemicals. *J. Catal.* **2023**, *424*, 1–8.

[69] Li, S. Q.; Wang, S. B.; Wang, Y. H.; He, J. H.; Li, K.; Xu, Y. J.; Wang, M. X.; Zhao, S. Y.; Li, X. N.; Zhong, X. et al. Doped Mn enhanced NiS electrooxidation performance of HMF into FDCA at industrial-level current density. *Adv. Funct. Mater.* **2023**, *33*, 2214488.

[70] Yang, Z. H.; Zhang, B. L.; Yan, C. Y.; Xue, Z. M.; Mu, T. C. The pivot to achieve high current density for biomass electrooxidation: Accelerating the reduction of Ni^{3+} to Ni^{2+}. *Appl. Catal. B: Environ.* **2023**, *330*, 122590.

[71] Zhao, Y. Y.; Cai, M. K.; Xian, J. H.; Sun, Y. M.; Li, G. Q. Recent advances in the electrocatalytic synthesis of 2,5-furandicarboxylic acid from 5-(hydroxymethyl)furfural. *J. Mater. Chem. A* **2021**, *9*, 20164–20183.

[72] Chen, C. L.; Wang, L. C.; Zhu, B.; Zhou, Z. Q.; El-Hout, S. I.; Yang, J.; Zhang, J. 2,5-Furandicarboxylic acid production via catalytic oxidation of 5-hydroxymethylfurfural: Catalysts, processes and reaction mechanism. *J. Energy Chem.* **2021**, *54*, 528–554.

[73] Pang, X. L.; Bai, H. Y.; Zhao, H. Q.; Fan, W. Q.; Shi, W. D. Efficient electrocatalytic oxidation of 5-hydroxymethylfurfural coupled with 4-nitrophenol hydrogenation in a water system. *ACS Catal.* **2022**, *12*, 1545–1557.

[74] Jiang, X. L.; Li, W.; Liu, Y. X.; Zhao, L.; Chen, Z. K.; Zhang, L.; Zhang, Y. G.; Yun, S. N. Electrocatalytic oxidation of 5-hydroxymethylfurfural for sustainable 2,5-furandicarboxylic acid production-from mechanism to catalysts design. *SusMat* **2023**, *3*, 21–43.

[75] Wu, J. C.; Kong, Z. J.; Li, Y. Y.; Lu, Y. X.; Zhou, P.; Wang, H. F.; Xu, L. T.; Wang, S. Y.; Zou, Y. Q. Unveiling the adsorption behavior and redox properties of PtNi nanowire for biomass-derived molecules electrooxidation. *ACS Nano* **2022**, *16*, 21518–21526.

[76] Xu, H.; Shang, H. Y.; Wang, C.; Du, Y. K. Low-dimensional metallic nanomaterials for advanced electrocatalysis. *Adv. Funct. Mater.* **2020**, *30*, 2006317.

[77] Liu, Y. L.; Zheng, Z. Y.; Jabeen, S.; Liu, N. Y.; Liu, Y. X.; Cheng, Y. Y.; Li, Y. X.; Yu, J. W.; Wu, X.; Yan, N. N. et al. Mechanochemical route to fabricate an efficient nitrate reduction electrocatalyst. *Nano Res.* **2024**, *17*, 4889–4897.

[78] Wu, T. Z.; Han, M. Y.; Xu, Z. C. J. Size effects of electrocatalysts: More than a variation of surface area. *ACS Nano* **2022**, *16*, 8531–8539.

[79] Zhou, A. W.; Wang, D. S.; Li, Y. D. Hollow microstructural regulation of single-atom catalysts for optimized electrocatalytic performance. *Microstructures* **2022**, *2*, 2022005.

[80] Wang, L. G.; Wu, J. B.; Wang, S. W.; Liu, H.; Wang, Y.; Wang, D. S. The reformation of catalyst: From a trial-and-error synthesis to rational design. *Nano Res.* **2024**, *17*, 3261–3301.

[81] Zhang, S.; Wang, R. Y.; Zhang, X.; Zhao, H. Recent advances in single-atom alloys: Preparation methods and applications in heterogeneous catalysis. *RSC Adv.* **2024**, *14*, 3936–3951.

[82] Li, L. L.; Zhao, Z. J.; Zhang, G.; Cheng, D. F.; Chang, X.; Yuan, X. T.; Wang, T.; Gong, J. L. Neural network accelerated investigation of the dynamic structure–performance relations of electrochemical CO_2 reduction over SnO_x surfaces. *Research* **2023**, *6*, 0067.

[83] Li, W. H.; Ye, B. C.; Yang, J. R.; Wang, Y.; Yang, C. J.; Pan, Y. M.; Tang, H. T.; Wang, D. S.; Li, Y. D. A single-atom cobalt catalyst for the fluorination of acyl chlorides at parts-per-million catalyst loading. *Angew. Chem., Int. Ed.* **2022**, *61*, e202209749.

[84] Wang, H. W.; Gu, X. K.; Zheng, X. S.; Pan, H. B.; Zhu, J. F.; Chen, S.; Cao, L. N.; Li, W. X.; Lu, J. L. Disentangling the size-dependent geometric and electronic effects of palladium nanocatalysts beyond selectivity. *Sci. Adv.* **2019**, *5*, eaat6413.

[85] Zhong, J.; Shen, Y. L.; Zhu, P.; Yao, S.; An, C. H. Size-effect on Ni electrocatalyst: The case of electrochemical benzyl alcohol oxidation. *Nano Res.* **2023**, *16*, 202–208.

[86] Liu, G. H.; Nie, T. Q.; Wang, H. J.; Shen, T. Y.; Sun, X. L.; Bai, S.; Zheng, L. R.; Song, Y. F. Size sensitivity of supported palladium species on layered double hydroxides for the electro-oxidation dehydrogenation of hydrazine: From nanoparticles to nanoclusters and single atoms. *ACS Catal.* **2022**, *12*, 10711–10717.

[87] Jin, T.; Han, Q. Q.; Wang, Y. J.; Jiao, L. F. 1D nanomaterials: Design, synthesis, and applications in sodium-ion batteries. *Small* **2018**, *14*, 1703086.

[88] Garnett, E.; Mai, L. Q.; Yang, P. D. Introduction: 1D nanomaterials/nanowires. *Chem. Rev.* **2019**, *119*, 8955–8957.

[89] Chen, F.; Yang, F.; Sheng, C.; Li, J. Z.; Xu, H.; Qing, Y.; Chen, S.; Wu, Y. Q.; Lu, X. H. Electronic structure modulation of nickel hydroxide porous nanowire arrays via manganese doping for urea-assisted energy-efficient hydrogen generation. *J. Colloid Interface Sci.* **2022**, *626*, 445–452.

[90] Mao, J. J.; Chen, W. X.; He, D. S.; Wan, J. W.; Pei, J. J.; Dong, J. C.; Wang, Y.; An, P. F.; Jin, Z.; Xing, W. et al. Design of ultrathin Pt-Mo-Ni nanowire catalysts for ethanol electrooxidation. *Sci. Adv.* **2017**, *3*, e1603068.

[91] Yu, Z. Y.; Lang, C. C.; Gao, M. R.; Chen, Y.; Fu, Q. Q.; Duan, Y.; Yu, S. H. Ni-Mo-O nanorod-derived composite catalysts for efficient alkaline water-to-hydrogen conversion via urea electrolysis. *Energy Environ. Sci.* **2018**, *11*, 1890–1897.

[92] Ning, S. B.; Ou, H. H.; Li, Y. G.; Lv, C. C.; Wang, S. F.; Wang, D. S.; Ye, J. H. Co^0–$Co^{\delta+}$ interface double-site-mediated C–C coupling for the photothermal conversion of CO_2 into light olefins. *Angew. Chem., Int. Ed.* **2023**, *62*, e202302253.

[93] Qiu, W. B.; Qin, S. M.; Li, Y. B.; Cao, N.; Cui, W. R.; Zhang, Z. D.; Zhuang, Z. C.; Wang, D. S.; Zhang, Y. Overcoming electrostatic interaction via pulsed electroreduction for boosting the electrocatalytic urea synthesis. *Angew. Chem., Int. Ed.* **2024**, *63*, e202402684.

[94] Zhang, Y. D.; Sun, Y. J.; Wang, Q. Y.; Zhuang, Z. C.; Ma, Z. T.; Liu, L. M.; Wang, G. M.; Wang, D. S.; Zheng, X. S. Synergy of photogenerated electrons and holes toward efficient photocatalytic urea synthesis from CO_2 and N_2. *Angew. Chem., Int. Ed.* **2024**, *63*, e202405637.

[95] Tan, C. L.; Cao, X. H.; Wu, X. J.; He, Q. Y.; Yang, J.; Zhang, X.; Chen, J. Z.; Zhao, W.; Han, S. K.; Nam, G. H. et al. Recent advances in ultrathin two-dimensional nanomaterials. *Chem. Rev.* **2017**, *117*, 6225–6331.

[96] Yang, J. R.; Zhu, C. X.; Wang, D. S. A simple organo-electrocatalysis system for the chlor-related industry. *Angew. Chem., Int. Ed.* **2024**, *63*, e202406883.

[97] Jiang, H.; Bu, S. Y.; Gao, Q. L.; Long, J.; Wang, P. F.; Lee, C. S.; Zhang, W. J. Ultrathin two-dimensional nickel-organic framework nanosheets for efficient electrocatalytic urea oxidation. *Mater. Today Energy* **2022**, *27*, 101024.

[98] Hao, J.; Liu, J. W.; Wu, D.; Chen, M. X.; Liang, Y.; Wang, Q.; Wang, L.; Fu, X. Z.; Luo, J. L. *In situ* facile fabrication of $Ni(OH)_2$ nanosheet arrays for electrocatalytic co-production of formate and hydrogen from methanol in alkaline solution. *Appl. Catal. B: Environ.* **2021**, *281*, 119510.

[99] Zhang, J. F.; Gong, W. B.; Yin, H. J.; Wang, D. D.; Zhang, Y. X.; Zhang, H. M.; Wang, G. Z.; Zhao, H. J. *In situ* growth of ultrathin $Ni(OH)_2$ nanosheets as catalyst for electrocatalytic oxidation reactions. *ChemSusChem* **2021**, *14*, 2935–2942.

[100] Zhu, Y. J.; Liu, C.; Cui, S. W.; Lu, Z. R.; Ye, J. Y.; Wen, Y. Z.; Shi, W. J.; Huang, X. X.; Xue, L. Y.; Bian, J. J. et al. Multistep dissolution of lamellar crystals generates superthin amorphous $Ni(OH)_2$ catalyst for UOR. *Adv. Mater.* **2023**, *35*, 2301549.

[101] Liu, N. Y.; Wu, R. Q.; Liu, Y. X.; Liu, Y. L.; Deng, P. J.; Li, Y. X.; Du, Y. C.; Cheng, Y. Y.; Zhuang, Z. C.; Kang, Z. H. et al. Oxygen vacancy engineering of Fe-doped $NiMoO_4$ for electrocatalytic N_2 fixation to NH_3. *Inorg. Chem.* **2023**, *62*, 11990–12000.

[102] Zhuang, C. Q.; Chang, Y.; Li, W. M.; Li, S. J.; Xu, P.; Zhang, H.; Zhang, Y. H.; Zhang, C.; Gao, J. F.; Chen, G. et al. Light-induced variation of lithium coordination environment in g-C_3N_4 nanosheet for highly efficient oxygen reduction reactions. *ACS Nano* **2024**, *18*, 5206–5217.

[103] Zhuang, C. Q.; Li, W. M.; Chang, Y.; Li, S. J.; Zhang, Y. H.; Li, Y. L.; Gao, J. F.; Chen, G.; Kang, Z. H. Coordination environment

dominated catalytic selectivity of photocatalytic hydrogen and oxygen reduction over switchable gallium and nitrogen active sites. *J. Mater. Chem. A* **2024**, *12*, 5711–5718.

[104] Lv, L. Y.; Tan, H.; Kong, Y.; Tang, B.; Ji, Q. Q.; Liu, Y. Y.; Wang, C.; Zhuang, Z. C.; Wang, H. J.; Ge, M. et al. Breaking the scaling relationship in C-N coupling via the doping effects for efficient urea electrosynthesis. *Angew. Chem., Int. Ed.* **2024**, *63*, e202401943.

[105] Gan, T.; Wang, D. S. Atomically dispersed materials: Ideal catalysts in atomic era. *Nano Res.* **2024**, *17*, 18–38.

[106] Qi, Z. J.; Zhou, Y.; Guan, R. N.; Fu, Y. S.; Baek, J. B. Tuning the coordination environment of carbon-based single-atom catalysts via doping with multiple heteroatoms and their applications in electrocatalysis. *Adv. Mater.* **2023**, *35*, 2210575.

[107] Wang, S. S.; Zhao, K.; Chen, Z.; Wang, L.; Qi, Z. H.; Hao, J. H.; Shi, W. D. New insights into cations effect in oxygen evolution reaction. *Chem. Eng. J.* **2022**, *433*, 133518.

[108] Wu, X.; Tong, Z.; Liu, Y. L.; Li, Y. X.; Cheng, Y. Y.; Yu, J. W.; Cao, P.; Zhuang, C. Q.; Shi, Q. Z.; Liu, N. Y. et al. Modification of the CuO electronic structure for enhanced selective electrochemical CO_2 reduction to ethylene. *Nano Res.* **2024**, *17*, 7194–7202.

[109] Zhao, C. X.; Wang, H. F.; Li, B. Q.; Zhang, Q. Multianion transition metal compounds: Synthesis, regulation, and electrocatalytic applications. *Acc. Mater. Res.* **2021**, *2*, 1082–1092.

[110] Wang, S. C.; Zhang, M. Y.; Mu, X. Q.; Liu, S. L.; Wang, D. S.; Dai, Z. H. Atomically dispersed multi-site catalysts: Bifunctional oxygen electrocatalysts boost flexible zinc-air battery performance. *Energy Environ. Sci.* **2024**, *17*, 4847–4870.

[111] Han, A. L.; Sun, W. M.; Wan, X.; Cai, D. D.; Wang, X. J.; Li, F.; Shui, J. L.; Wang, D. S. Construction of Co_4 atomic clusters to enable Fe-N_4 motifs with highly active and durable oxygen reduction performance. *Angew. Chem., Int. Ed.* **2023**, *62*, e202303185.

[112] Zhang, Y. F.; Liu, L. S.; Li, Y. X.; Mu, X. Q.; Mu, S. C.; Liu, S. L.; Dai, Z. H. Strong synergy between physical and chemical properties: Insight into optimization of atomically dispersed oxygen reduction catalysts. *J. Energy Chem.* **2024**, *91*, 36–49.

[113] Zhang, A.; Liang, Y. X.; Zhang, H.; Geng, Z. G.; Zeng, J. Doping regulation in transition metal compounds for electrocatalysis. *Chem. Soc. Rev.* **2021**, *50*, 9817–9844.

[114] Liu, Y. L.; Zhuang, Z. C.; Liu, Y. X.; Liu, N. Y.; Li, Y. X.; Cheng, Y. Y.; Yu, J. W.; Yu, R. H.; Li, H. T.; Wang, D. S. Shear-strained Pd single-atom electrocatalysts for nitrate reduction to ammonia. *Angew. Chem., Int. Ed.* **2024**, *63*, e202411396.

[115] Wang, J.; Teschner, D.; Yao, Y. Y.; Huang, X.; Willinger, M.; Shao, L. D.; Schlögl, R. Fabrication of nanoscale NiO/Ni heterostructures as electrocatalysts for efficient methanol oxidation. *J. Mater. Chem. A* **2017**, *5*, 9946–9951.

[116] Guan, S. Y.; Yuan, Z. L.; Zhuang, Z. C.; Zhang, H. H.; Wen, H.; Fan, Y. P.; Li, B. J.; Wang, D. S.; Liu, B. Z. Why do single-atom alloys catalysts outperform both single-atom catalysts and nanocatalysts on MXene. *Angew. Chem., Int. Ed.* **2024**, *63*, e202316550.

[117] Yang, J. R.; Zhu, C. X.; Li, W. H.; Zheng, X. S.; Wang, D. S. Organocatalyst supported by a single-atom support accelerates both electrodes used in the chlor-alkali industry via modification of non-covalent interactions. *Angew. Chem., Int. Ed.* **2024**, *63*, e202314382.

[118] Wang, X. Y.; Pan, Y. Z.; Yang, J. R.; Li, W. H.; Gan, T.; Pan, Y. M.; Tang, H. T.; Wang, D. S. Single-atom iron catalyst as an advanced redox mediator for anodic oxidation of organic electrosynthesis. *Angew. Chem., Int. Ed.* **2024**, *63*, e202404295.

[119] Tao, Y.; Guan, J. P.; Zhang, J.; Hu, S. Y.; Ma, R. Z.; Zheng, H. R.; Gong, J. X.; Zhuang, Z. C.; Liu, S. J.; Ou, H. H. et al. Ruthenium single atomic sites surrounding the support pit with exceptional photocatalytic activity. *Angew. Chem., Int. Ed.* **2024**, *63*, e202400625.

[120] Zhu, C. X.; Yang, J. R.; Zhang, J. W.; Wang, X. Q.; Gao, Y.; Wang, D. S.; Pan, H. G. Single-atom materials: The application in energy conversion. *Interdiscip. Mater.* **2024**, *3*, 74–86.

[121] Liang, X.; Fu, N. H.; Yao, S. C.; Li, Z.; Li, Y. D. The progress and outlook of metal single-atom-site catalysis. *J. Am. Chem. Soc.* **2022**, *144*, 18155–18174.

[122] Wang, S. W.; Wang, L. G.; Wang, D. S.; Li, Y. D. Recent advances of single-atom catalysts in CO_2 conversion. *Energy Environ. Sci.* **2023**, *16*, 2759–2803.

[123] Zhang, Z. D.; Zhu, J. X.; Chen, S. H.; Sun, W. M.; Wang, D. S. Liquid fluxional Ga single atom catalysts for efficient electrochemical CO_2 reduction. *Angew. Chem., Int. Ed.* **2023**, *62*, e202215136.

[124] Chen, S. H.; Ye, C. L.; Wang, Z. W.; Li, P.; Jiang, W. J.; Zhuang, Z. C.; Zhu, J. X.; Zheng, X. B.; Zaman, S.; Ou, H. H. et al. Selective CO_2 reduction to ethylene mediated by adaptive small-molecule engineering of copper-based electrocatalysts. *Angew. Chem., Int. Ed.* **2023**, *62*, e202315621.

[125] Tang, H. T.; Zhou, H. Y.; Pan, Y. M.; Zhang, J. L.; Cui, F. H.; Li, W. H.; Wang, D. S. Single-atom manganese-catalyzed oxygen evolution drives the electrochemical oxidation of silane to silanol. *Angew. Chem., Int. Ed.* **2024**, *63*, e202315032.

[126] Chen, Y. J.; Jiang, B.; Hao, H. G.; Li, H. J.; Qiu, C. Y.; Liang, X.; Qu, Q. Y.; Zhang, Z. D.; Gao, R.; Duan, D. M. et al. Atomic-level regulation of cobalt single-atom nanozymes: Engineering high-efficiency catalase mimics. *Angew. Chem., Int. Ed.* **2023**, *62*, e202301879.

[127] Hu, Y. M.; Chao, T. T.; Li, Y. P.; Liu, P. G.; Zhao, T. H.; Yu, G.; Chen, C.; Liang, X.; Jin, H. L.; Niu, S. W. et al. Cooperative Ni(Co)-Ru-P sites activate dehydrogenation for hydrazine oxidation assisting self-powered H_2 production. *Angew. Chem., Int. Ed.* **2023**, *62*, e202308800.

[128] Ma, G.; Zhang, X. Y.; Zhou, G. F.; Wang, X. Hydrogen production from methanol reforming electrolysis at NiO nanosheets supported Pt nanoparticles. *Chem. Eng. J.* **2021**, *411*, 128292.

[129] Wu, Q.; Gao, Q. P.; Sun, L. M.; Guo, H. M.; Tai, X. S.; Li, D.; Liu, L.; Ling, C. Y.; Sun, X. P. Facilitating active species by decorating CeO_2 on Ni_3S_2 nanosheets for efficient water oxidation electrocatalysis. *Chin. J. Catal.* **2021**, *42*, 482–489.

[130] Sun, Y.; Wang, J.; Qi, Y. F.; Li, W. J.; Wang, C. Efficient electrooxidation of 5-hydroxymethylfurfural using Co-doped Ni_3S_2 catalyst: Promising for H_2 production under industrial-level current density. *Adv. Sci.* **2022**, *9*, 2200957.

[131] Wang, H. N.; Guan, A. X.; Zhang, J. B.; Mi, Y. Y.; Li, S.; Yuan, T. T.; Jing, C.; Zhang, L. J.; Zhang, L. J.; Zheng, G. F. Copper-doped nickel oxyhydroxide for efficient electrocatalytic ethanol oxidation. *Chin. J. Catal.* **2022**, *43*, 1478–1484.

[132] Wang, L. P.; Zhu, Y. J.; Wen, Y. Z.; Li, S. Y.; Cui, C. Y.; Ni, F. L.; Liu, Y. X.; Lin, H. P.; Li, Y. Y.; Peng, H. S. et al. Regulating the local charge distribution of Ni active sites for the urea oxidation reaction. *Angew. Chem., Int. Ed.* **2021**, *60*, 10577–10582.

[133] Qin, H. Y.; Ye, Y. K.; Li, J. H.; Jia, W. Q.; Zheng, S. Y.; Cao, X. J.; Lin, G. L.; Jiao, L. F. Synergistic engineering of doping and vacancy in $Ni(OH)_2$ to boost urea electrooxidation. *Adv. Funct. Mater.* **2023**, *33*, 2209698.

[134] Zhao, K.; Yang, W. S.; Li, L. H.; Wang, S. S.; Wang, L.; Qi, Z. H.; Yang, Y. G.; Chen, Z.; Zhuang, J. W.; Hao, J. H. et al. Discharge induced-activation of phosphorus-doped nickel oxyhydroxide for oxygen evolution reaction. *Chem. Eng. J.* **2022**, *435*, 135049.

[135] Zhang, L. L.; Chang, Q. W.; Chen, H. M.; Shao, M. H. Recent advances in palladium-based electrocatalysts for fuel cell reactions and hydrogen evolution reaction. *Nano Energy* **2016**, *29*, 198–219.

[136] Lei, H.; Ma, L.; Wan, Q. X.; Tan, S. Z.; Yang, B.; Wang, Z. L.; Mai, W. J.; Fan, H. J. Promoting surface reconstruction of NiFe layered double hydroxide for enhanced oxygen evolution. *Adv. Energy Mater.* **2022**, *12*, 2202522.

[137] Zhu, X. J.; Dou, X. Y.; Dai, J.; An, X. D.; Guo, Y. Q.; Zhang, L. D.; Tao, S.; Zhao, J. Y.; Chu, W. S.; Zeng, X. C. et al. Metallic nickel

hydroxide nanosheets give superior electrocatalytic oxidation of urea for fuel cells. *Angew. Chem., Int. Ed.* **2016**, *55*, 12465–12469.

[138] Xu, X. F.; Ullah, H.; Humayun, M.; Li, L. F.; Zhang, X.; Bououdina, M.; Debecker, D. P.; Huo, K. F.; Wang, D. L.; Wang, C. D. Fluorinated Ni–O–C heterogeneous catalyst for efficient urea-assisted hydrogen production. *Adv. Funct. Mater.* **2023**, *33*, 2303986.

[139] Yang, S. X.; Xiang, X. P.; He, Z. Y.; Zhong, W. Y.; Jia, C. H.; Gong, Z. H.; Zhang, N.; Zhao, S. J.; Chen, Y. Anionic defects engineering of $NiCo_2O_4$ for 5-hydroxymethylfurfural electrooxidation. *Chem. Eng. J.* **2023**, *457*, 141344.

[140] Xie, H.; Feng, Y. F.; He, X. Y.; Zhu, Y.; Li, Z. Y.; Liu, H. H.; Zeng, S. Y.; Qian, Q. Z.; Zhang, G. Q. Construction of nitrogen-doped biphasic transition-metal sulfide nanosheet electrode for energy-efficient hydrogen production via urea electrolysis. *Small* **2023**, *19*, 2207425.

[141] Mu, X. Q.; Liu, S. L.; Zhang, M. Y.; Zhuang, Z. C.; Chen, D.; Liao, Y. R.; Zhao, H. Y.; Mu, S. C.; Wang, D. S.; Dai, Z. H. Symmetry-broken Ru nanoparticles with parasitic Ru-Co dual-single atoms overcome the volmer step of alkaline hydrogen oxidation. *Angew. Chem., Int. Ed.* **2024**, *63*, e202319618.

[142] Wang, Y.; Wu, J.; Tang, S. H.; Yang, J. R.; Ye, C. L.; Chen, J.; Lei, Y. P.; Wang, D. S. Synergistic Fe–Se atom pairs as bifunctional oxygen electrocatalysts boost low-temperature rechargeable Zn-air battery. *Angew. Chem., Int. Ed.* **2023**, *62*, e202219191.

[143] Qiao, S. C.; Shou, H. W.; Xu, W. J.; Cao, Y. Y.; Zhou, Y. Z.; Wang, Z. X.; Wu, X. J.; He, Q.; Song, L. Regulating and identifying the structures of PdAu alloys with splendid oxygen reduction activity for rechargeable zinc-air batteries. *Energy Environ. Sci.* **2023**, *16*, 5842–5851.

[144] Ji, Z. J.; Song, Y. J.; Zhao, S. H.; Li, Y.; Liu, J.; Hu, W. P. Pathway manipulation via Ni, Co, and V ternary synergism to realize high efficiency for urea electrocatalytic oxidation. *ACS Catal.* **2022**, *12*, 569–579.

[145] Wang, P. T.; Bai, X. W.; Jin, H. Y.; Gao, X. T.; Davey, K.; Zheng, Y.; Jiao, Y.; Qiao, S. Z. Directed urea-to-nitrite electrooxidation via tuning intermediate adsorption on Co, Ge Co-doped Ni sites. *Adv. Funct. Mater.* **2023**, *33*, 2300687.

[146] Feng, C.; Lv, M. Y.; Shao, J. X.; Wu, H. Y.; Zhou, W. L.; Qi, S.; Deng, C.; Chai, X. Y.; Yang, H. P.; Hu, Q. et al. Lattice strain engineering of Ni_2P enables efficient catalytic hydrazine oxidation-assisted hydrogen production. *Adv. Mater.* **2023**, *35*, 2305598.

[147] Zhou, S. Q.; Zhao, Y. X.; Shi, R.; Wang, Y. C.; Ashok, A.; Héraly, F.; Zhang, T.; Yuan, J. Y. Vacancy-rich MXene-immobilized Ni single atoms as a high-performance electrocatalyst for the hydrazine oxidation reaction. *Adv. Mater.* **2022**, *34*, 2204388.

[148] Yang, M.; Liu, Y. Y.; Ge, W. Y.; Liu, Z. R. Enhanced electrocatalytic activity of sulfur and tungsten Co-doped nickel hydroxide nanosheets for urea oxidation. *Colloids Surf. A: Physicochem. Eng. Aspects* **2023**, *665*, 131226.

[149] Kim, M.; Min, K.; Ko, D.; Seong, H.; Shim, S. E.; Baeck, S. H. Regulating the electronic structure of Ni_2P by one-step Co, N dual-doping for boosting electrocatalytic performance toward oxygen evolution reaction and urea oxidation reaction. *J. Colloid Interface Sci.* **2023**, *650*, 1851–1861.

[150] Wang, W. X.; Xiong, F. Y.; Zhu, S. H.; Chen, J. H.; Xie, J.; An, Q. Y. Defect engineering in molybdenum-based electrode materials for energy storage. *eScience* **2022**, *2*, 278–294.

[151] Guo, D. X.; Wang, S.; Xu, J.; Zheng, W. J.; Wang, D. H. Defect and interface engineering for electrochemical nitrogen reduction reaction under ambient conditions. *J. Energy Chem.* **2022**, *65*, 448–468.

[152] Xiao, H. B.; Chi, K.; Yin, H. X.; Zhou, X. J.; Lei, P. X.; Liu, P. Z.; Fang, J. K.; Li, X. H.; Yuan, S. L.; Zhang, Z. et al. Excess activity tuned by distorted tetrahedron in $CoMoO_4$ for oxygen evolution. *Energy Environ. Mater.* **2022**, *7*, e12495.

[153] Zheng, Y. F.; Fu, K. X.; Yu, Z. H.; Su, Y.; Han, R.; Liu, Q. L. Oxygen vacancies in a catalyst for VOCs oxidation: Synthesis, characterization, and catalytic effects. *J. Mater. Chem. A* **2022**, *10*, 14171–14186.

[154] Sun, K. S.; Pang, J. X.; Zheng, Y.; Xing, F. Y.; Jiang, R.; Min, J.; Ye, J. H.; Wang, L. P.; Luo, Y.; Gu, T. T. et al. Oxygen vacancies enriched MOF-derived MnO/C hybrids for high-performance aqueous zinc ion battery. *J. Alloys Compd.* **2022**, *923*, 166470.

[155] Yu, X.; Hu, C. W.; Ji, P. X.; Ren, Y. M.; Zhao, H. Y.; Liu, G.; Xu, R.; Zhu, X. D.; Li, Z. Q.; Ma, Y. Q. et al. Optically transparent ultrathin NiCo alloy oxide film: Precise oxygen vacancy modulation and control for enhanced electrocatalysis of water oxidation. *Appl. Catal. B: Environ.* **2022**, *310*, 121301.

[156] Gong, Z. H.; Zhong, W. Y.; He, Z. Y.; Liu, Q. Y.; Chen, H. J.; Zhou, D.; Zhang, N.; Kang, X. W.; Chen, Y. Regulating surface oxygen species on copper(I) oxides via plasma treatment for effective reduction of nitrate to ammonia. *Appl. Catal. B: Environ.* **2022**, *305*, 121021.

[157] Rao, P.; Wu, D. X.; Wang, T. J.; Li, J.; Deng, P. L.; Chen, Q.; Shen, Y. J.; Chen, Y.; Tian, X. L. Single atomic cobalt electrocatalyst for efficient oxygen reduction reaction. *eScience* **2022**, *2*, 399–404.

[158] Li, Z.; Zhang, Y.; Feng, Y.; Cheng, C. Q.; Qiu, K. W.; Dong, C. K.; Liu, H.; Du, X. W. Co_3O_4 nanoparticles with ultrasmall size and abundant oxygen vacancies for boosting oxygen involved reactions. *Adv. Funct. Mater.* **2019**, *29*, 1903444.

[159] Tong, Y.; Chen, P. Z.; Zhang, M. X.; Zhou, T. P.; Zhang, L. D.; Chu, W. S.; Wu, C. Z.; Xie, Y. Oxygen vacancies confined in nickel molybdenum oxide porous nanosheets for promoted electrocatalytic urea oxidation. *ACS Catal.* **2018**, *8*, 1–7.

[160] Liu, J. B.; Tao, S. Y. Laser Promoting oxygen vacancies generation in alloy via Mo for HMF electrochemical oxidation. *Adv. Sci.* **2023**, *10*, 2302641.

[161] Peng, L. S.; Yang, N.; Yang, Y. Q.; Wang, Q.; Xie, X. Y.; Sun-Waterhouse, D.; Shang, L.; Zhang, T. R.; Waterhouse, G. I. N. Atomic cation-vacancy engineering of NiFe-layered double hydroxides for improved activity and stability towards the oxygen evolution reaction. *Angew. Chem., Int. Ed.* **2021**, *60*, 24612–24619.

[162] Ge, J. J.; Zheng, J. Y.; Zhang, J. W.; Jiang, S. Y.; Zhang, L. L.; Wan, H.; Wang, L. M.; Ma, W.; Zhou, Z.; Ma, R. Z. Controllable atomic defect engineering in layered $Ni_xFe_{1-x}(OH)_2$ nanosheets for electrochemical overall water splitting. *J. Mater. Chem. A* **2021**, *9*, 14432–14443.

[163] Han, W. K.; Wei, J. X.; Xiao, K.; Ouyang, T.; Peng, X. W.; Zhao, S. L.; Liu, Z. Q. Activating lattice oxygen in layered lithium oxides through cation vacancies for enhanced urea electrolysis. *Angew. Chem., Int. Ed.* **2022**, *61*, e202206050.

[164] Qi, Y. F.; Wang, K. Y.; Sun, Y.; Wang, J.; Wang, C. Engineering the electronic structure of NiFe layered double hydroxide nanosheet array by implanting cationic vacancies for efficient electrochemical conversion of 5-hydroxymethylfurfural to 2,5-furandicarboxylic acid. *ACS Sustainable Chem. Eng.* **2022**, *10*, 645–654.

[165] Zheng, J. X.; Peng, X. F.; Xu, Z.; Gong, J. B.; Wang, Z. Cationic defect engineering in spinel $NiCo_2O_4$ for enhanced electrocatalytic oxygen evolution. *ACS Catal.* **2022**, *12*, 10245–10254.

[166] Luo, M. H.; Sun, W. P.; Xu, B. B.; Pan, H. G.; Jiang, Y. Z. Interface engineering of air electrocatalysts for rechargeable zinc-air batteries. *Adv. Energy Mater.* **2021**, *11*, 2002762.

[167] Lu, Y. X.; Dong, C. L.; Huang, Y. C.; Zou, Y. Q.; Liu, Y. B.; Li, Y. Y.; Zhang, N. N.; Chen, W.; Zhou, L.; Lin, H. Z. et al. Hierarchically nanostructured NiO-Co_3O_4 with rich interface defects for the electro-oxidation of 5-hydroxymethylfurfural. *Sci. China Chem.* **2020**, *63*, 980–986.

[168] Zeng, M.; Wu, J. H.; Li, Z. Y.; Wu, H. H.; Wang, J. L.; Wang, H. L.; He, L.; Yang, X. J. Interlayer effect in NiCo layered double hydroxide for promoted electrocatalytic urea oxidation. *ACS Sustainable Chem. Eng.* **2019**, *7*, 4777–4783.

[169] Zhou, Q. X.; Xu, C. X.; Hou, J. G.; Ma, W. Q.; Jian, T. Z.; Yan, S. S.; Liu, H. Duplex interpenetrating-phase FeNiZn and $FeNi_3$

heterostructure with low-Gibbs free energy interface coupling for highly efficient overall water splitting. *Nano-Micro Lett.* **2023**, *15*, 95.

[170] Liu, Y.; Xing, Y. Y.; Xu, S. J.; Lu, Y. K.; Sun, S. C.; Jiang, D. L. Interfacing Co_3Mo with $CoMoO_x$ for synergistically boosting electrocatalytic hydrogen and oxygen evolution reactions. *Chem. Eng. J.* **2022**, *431*, 133240.

[171] Zhou, H. B.; Zhang, D. X.; Dong, W. X.; Zhou, C. X.; Jiang, T. Y.; Liu, Y. S.; Tian, C. G.; Liu, Y. H.; Liu, Y.; Mao, B. D. Stainless steel mesh-based $CoSe/Ni_3Se_4$ heterostructure for efficient electrocatalytic overall water splitting. *Int. J. Hydrogen Energy* **2023**, *48*, 14554–14564.

[172] Liu, N. Y.; Liu, Y. X.; Liu, Y. L.; Li, Y. X.; Cheng, Y. Y.; Li, H. T. Modulation of photogenerated holes for enhanced photoelectrocatalytic performance. *Microstructures* **2023**, *3*, 2023001.

[173] He, C. H.; Liu, Q. Q.; Wang, H. M.; Xia, C. F.; Li, F. M.; Guo, W.; Xia, B. Y. Regulating reversible oxygen electrocatalysis by built-in electric field of heterojunction electrocatalyst with modified d-band. *Small* **2023**, *19*, 2207474.

[174] Tong, Z.; Liu, Y. L.; Wu, X.; Cheng, Y. Y.; Yu, J. W.; Zhang, X. Y.; Liu, N. Y.; Liu, X.; Li, H. T. Carbon quantum dots/Cu_2O photocatalyst for room temperature selective oxidation of benzyl alcohol. *Nanomaterials,* **2024**, *14*, 212.

[175] Zheng, D.; Yu, L. H.; Liu, W. X.; Dai, X. J.; Niu, X. X.; Fu, W. Q.; Shi, W. H.; Wu, F. F.; Cao, X. H. Structural advantages and enhancement strategies of heterostructure water-splitting electrocatalysts. *Cell Rep. Phys. Sci.* **2021**, *2*, 100443.

[176] Qi, Y. B.; Zhang, Y.; Yang, L.; Zhao, Y. H.; Zhu, Y. H.; Jiang, H. L.; Li, C. Z. Insights into the activity of nickel boride/nickel heterostructures for efficient methanol electrooxidation. *Nat. Commun.* **2022**, *13*, 4602.

[177] Qian, Q. Z.; Zhang, J. H.; Li, J. M.; Li, Y. P.; Jin, X.; Zhu, Y.; Liu, Y.; Li, Z. Y.; El-Harairy, A.; Xiao, C. et al. Artificial heterointerfaces achieve delicate reaction kinetics towards hydrogen evolution and hydrazine oxidation catalysis. *Angew. Chem., Int. Ed.* **2021**, *60*, 5984–5993.

[178] Luo, R. P.; Li, Y. Y.; Xing, L. X.; Wang, N.; Zhong, R. Y.; Qian, Z. Y.; Du, C. Y.; Yin, G. P.; Wang, Y. C.; Du, L. A dynamic $Ni(OH)_2$-NiOOH/NiFeP heterojunction enabling high-performance E-upgrading of hydroxymethylfurfural. *Appl. Catal. B: Environ.* **2022**, *311*, 121357.